공학석사 학위논문

Discrete Element Modeling of Anisotropic Mechanical Behaviors for Transversely Isotropic Rock

개별요소법을 이용한 횡등방성 암석의 역학적 이방성 모사

2013 년 2 월

서울대학교 대학원

에너지시스템공학부

박 보 나

Discrete Element Modeling of Anisotropic Mechanical Behaviors for Transversely Isotropic Rock

지도 교수 민 기 복

이 논문을 공학석사 학위논문으로 제출함
2013 년 2 월

서울대학교 대학원
에너지시스템공학부
박 보 나

박보나의 공학석사 학위논문을 인준함
2013 년 2 월

위 원 장 전 석 원 (인)

부위원장 민 기 복 (인)

위 원 송 재 준 (인)

Abstract

Discrete Element Modeling of Anisotropic Mechanical Behaviors for Transversely Isotropic Rock

Bona Park

Department of Energy Systems Engineering

Rock Mechanics & Rock Engineering Laboratory

The Graduate School

Seoul National University

Discrete Element Model is now recognized as a powerful tool for simulating mechanical behaviors of rock. In particular, bonded particle model has been successfully applied in emulating the elastic modulus, Poisson's ratio and strength parameters of rock by controlling the micro parameters of DEM. Although the consideration of anisotropy is important in many rock mechanics applications, DEM still remains as a tool for modeling an isotropic rock. In this study, DEM modeling was performed in order to represent the transversely isotropic rock such as shale and schist. The Smooth Joint Model was assigned to represent the bedding planes in order to form the transversely isotropic rock. DEM model was verified using the transformation of compliance tensor in transversely isotropic rock containing one set of fractures. Verification with respect to the strength anisotropy also resulted in good agreement with analytical model. It is demonstrated that the microparameters of smooth joint model were shown to contribute significantly to the anisotropic mechanical behaviors. Particle size sensitivity analysis was carried out and it was confirmed that using sufficiently high resolution is one of the key factors that can lead to more accurate DEM

modeling. The bonded particle model with smooth joints model can provide a competent tool for simulating the elastic modulus of transversely isotropic rock as long as it maintains a reasonable resolution.

Three different types of transversely isotropic rock were reproduced as DEM models and the properties of Asan gneiss, Boryeong shale and Yeoncheon schist (Cho *et al.*, 2012) were used as a reference for transversely isotropic rock modeling. To determine the microproperties of smooth joint model, the equivalent continuum model was used in order to obtain the normal and shear stiffness of weak plane. Bedding planes and foliations are generally smooth so the dilation angle (ψ) was regarded as 0^o. It is reasonable to choose the tensile strength of smooth joints as the value less than Brazilian tensile strength with the inclined angle of 0^o. Finally, cohesion and friction coefficient were estimated through iterative process. The strength and elastic modulus of transversely isotropic model varied with respect to the orientation of the smooth joints and the overall trends were similar to the laboratory experiments in Asan gneiss, Boryeong shale and Yeoncheon schist. BTS of the transversely isotropic model with high resolution seems to have good agreement with the laboratory results, however, it tended to be higher than actual value and this has been identified as the inherent limitations. In spite of the issues such as higher tensile strength in strong rock, the DEM model of transversely isotropic rock seems to model the strength and elastic behavior of the transversely isotropic rock to a reasonable extent.

After failure, fractures on DEM model were compared with broken rock specimen and the failure mechanism was analyzed. Based on the experimental study on layered rock (Abbass and André, 2010), the portion of layer fracture and central fracture length on Boryeong shale was measured and it was analyzed that the strength and failure mechanism containing high portion of layered fractures were dominated by the shear and /or tensile strength of the layers. By counting the number of micro tensile/shear cracks in DEM model, failure patterns were investigated.

This discrete element modeling in anisotropic rock is expected to pave the way for wide variety of engineering applications such as hydraulic

fracturing for shale gas production and wellbore stability analysis.

Keywords: Discrete Element Method, Smooth Joint Model, Transversely Isotropy, Wellbore Stability, Hydraulic Fracturing

Student Number: 2011 - 21095

Contents

Lists of Tables

Lists of Figures

Chapter 1. Introduction

1.1 Transverse Isotropy of Rock

Rock is generally anisotropic in nature. There are two types of anisotropic rocks: class A and class B (Barla, 1974). Class A rocks show anisotropic behavior without clear anisotropic formations such as joint sets, whereas class B rocks are composed of layers or beds that contribute to different mechanical properties depending on the direction. Most clsaa B rocks are a combination of intact rock, usually considered as an isotropic material, and one or two sets of parallel discontinuities or layers, which act as transversely isotropic or orthotropic planes depending upon the types of anisotropic model. Shale, gneiss, and schist can be classified as class B which have visible bedding, foliation and schistosity planes, and they are regarded as transversely isotropic rock as illustrated in Figure 1.1.

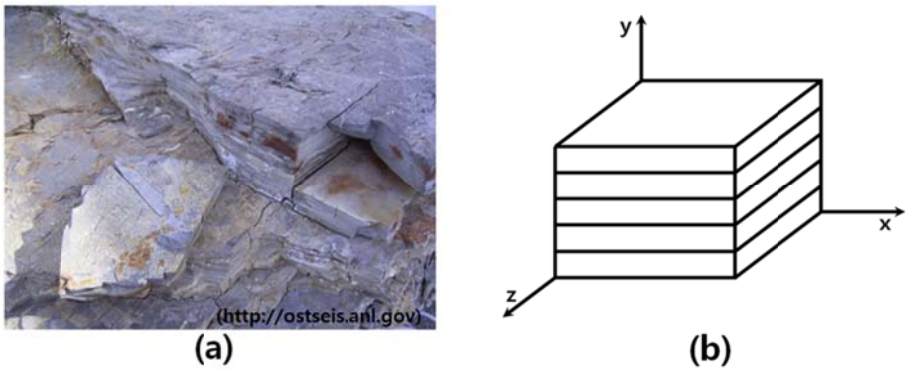

Figure 1.1: (a) Shale with bedding planes (U.S. department of the interior, bureau of land management, 2011), and (b) formation of transversely isotropic rock

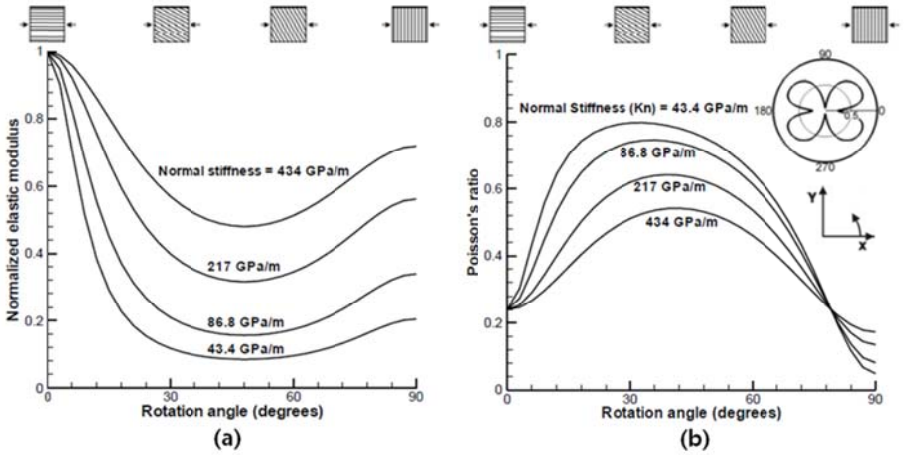

Figure 1.2: Variation of (a) normalized elastic moduli, and (b) Poisson's ratio with respect to the rotation of axes with different stiffness ratio by the analytic solutions (Min and Jing, 2004)

The anisotropic mechanical behaviors of transversely isotropic rock are shown in Figure 1.2 as the variation of elastic constants with respect to the rotation of axes. Values of elastic constants with different stiffness ratios were calculated and plotted using analytic solution (Min and Jing, 2004). Elastic moduli are normalized with respect to the value of intact rock in which the elastic modulus of rock with weak planes parallel to the loading direction is actually the same as that of intact rock. The rock with an inclined angle of 0^o has the least effect of anisotropy in terms of elastic modulus. The Poisson's ratio of transversely isotropic rock can exceed 0.5, which is the theoretical upper bound of Poisson's ratio for isotropic rock. The variation of elastic constants demonstrates that the consideration of anisotropy is important in rock mechanics applications, because the rock behavior is likely to be influenced by the angle of weak planes.

Direction-dependent mechanical behavior can be observed not only in the analytic solution but also from the results of laboratory experiments. According to the experimental results of Asan gneiss, Boryeong shale, and Yeoncheon schist (Cho *et al*., 2012), three sets of seven cylindrical specimens were cored with inclined angles of 0°, 15°, 30°, 45°, 60°, 75°, and 90° with respect to one set of discontinuities. Seven different cylindrical specimens are depicted in Figure 1.3. The elastic modulus variation, uniaxial compressive strength and Brazilian tensile strength in terms of inclined angles are plotted in Figures 1.4 and 1.5.

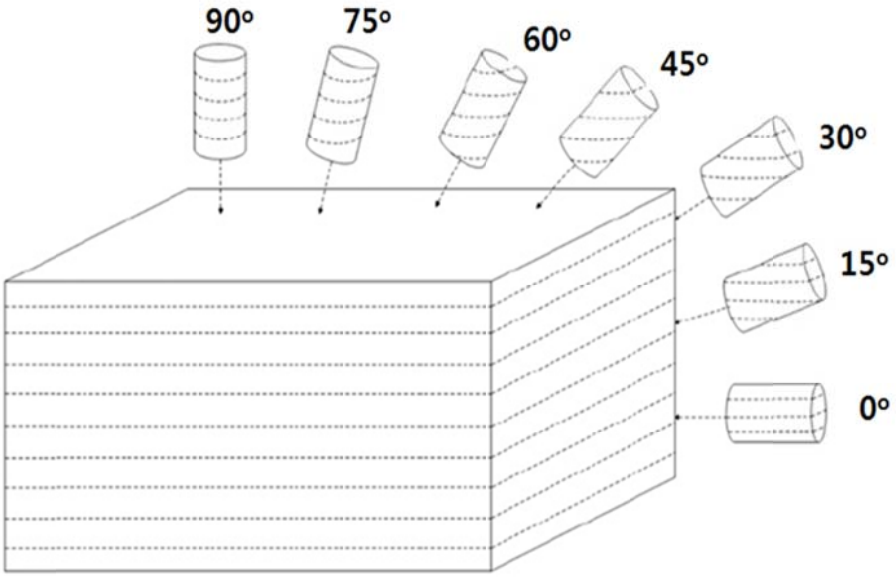

Figure 1.3: Seven cylindrical specimens with inclined angles (β) 0°, 15°, 30°, 45°, 60°, 75°, and 90° with respect to one set of transversely isotropic plane (Cho *et al.*, 2012)

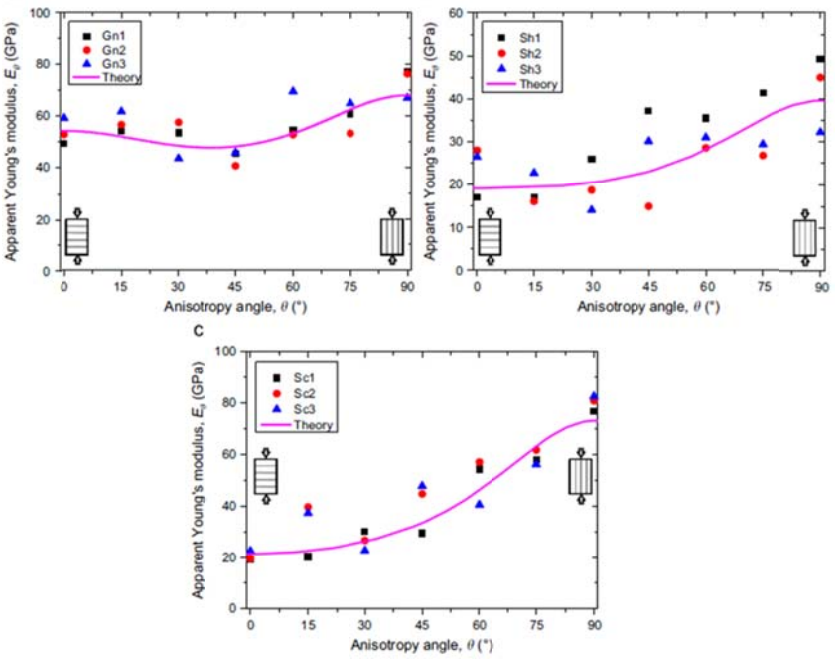

(a) Elastic modulus

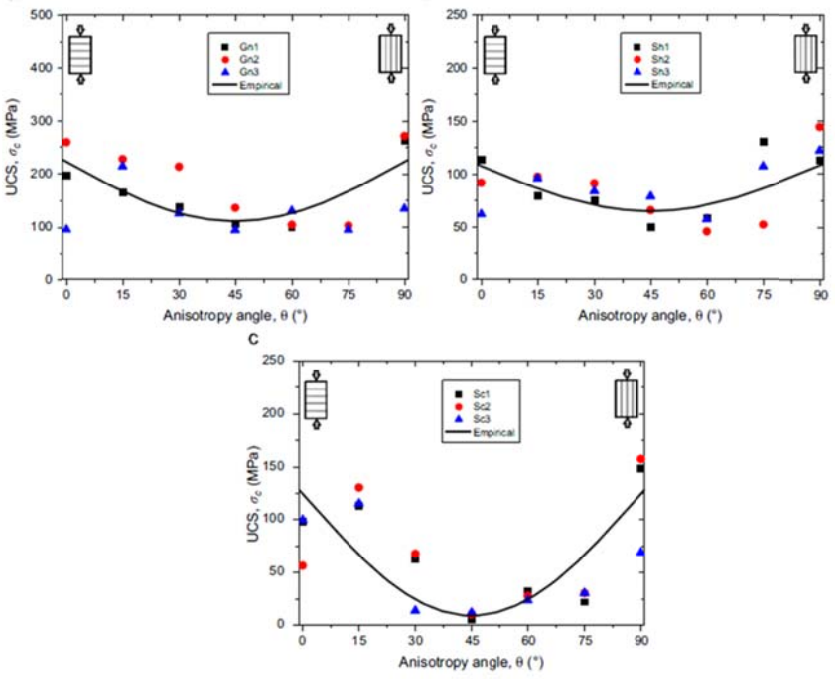

(b) Uniaxial compressive strength

Figure 1.4: Variation of anisotropic mechanical behaviors of Asan gneiss (top left), Boryeong shale (top right), and Yeoncheon schist (bottom) (Cho *et al.*, 2012) (Continued)

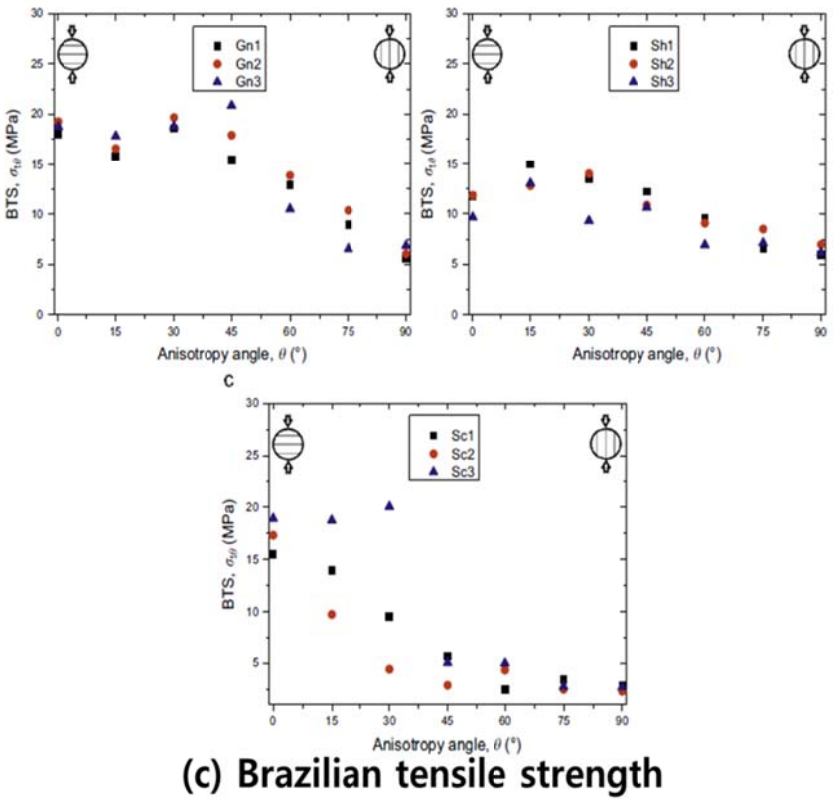

Figure 1.5: Variation of anisotropic mechanical behaviors of Asan gneiss (top left), Boryeong shale (top right), and Yeoncheon schist (bottom) (Cho *et al.*, 2012)

The results indicate that the anisotropic mechanical behaviors in transversely isotropic rock can also be captured by performing laboratory experiments. In order to model a transversely isotropic rock, the mechanical properties of Asan gneiss, Boryeong shale and Yeoncheon schist in Figures 1.4 and 1.5 were used as a reference. Modeling of anisotropic rock is important for shale gas production, because shale is shown to have a significant anisotropy in terms of elastic constants and compressive and tensile strength due to its bedding planes. The deformability and strength of shale is greatly affected by both the geometries and mechanical properties of

bedding planes. Therefore, transversely isotropic rock, the simplest type of anisotropy, was taken into account in this study. This anisotropic rock was reproduced as a numerical model through the discrete element method and it will be the first step for conducting an anisotropic analysis in rock engineering applications. In the Oseberg oil field in North Sea in the late 1990's, inclined borehole was severely damaged in the sedimentary rock formation (Okland *et al.*, 1998). As shown in Figure 1.6, borehole damaged with the inclined angle of 90^{o}. Theoretical failure criterion for isotropic rock failed to match the experienced results, because the anisotropy of rock was not considered. If the transversely isotropic model had been applied for wellbore stability analysis, then severe damage of the borehole might have been prevented. Thus, the consideration of rock anisotropy is important for simulating many rock engineering applications.

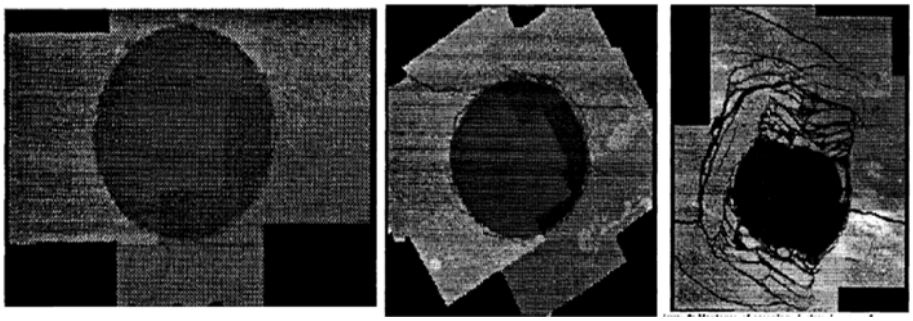

Figure 1.6: Images of cross-sections of shale samples, unloaded from 20 MPa external pressure. The inclined angle of 90^{o} (left), 10^{o} (middle) and 0^{o} (right) (Okland *et al.*, 1998)

1.2 Discrete Element Method

Discrete element method can be classified into two depending upon the shape of rigid body: the particulate system and the blocky system (Jing and Stephansson, 2007). This section focuses on the particulate system, because the numerical modeling in this study was performed through bonded particle model.

The Discrete Element Method (DEM) can describe the mechanical behavior of granular materials consisting of assemblies of discs or spheres. All particles are distinct rigid bodies, so that they can be completely detached and can interact to each other at their contact points. Some characteristics, advantages, and disadvantages of DEM are listed below (Cundall, 2001; Potyondy and Cundall, 2004; Itasca, 2008):

(a) DEM can model the granular materials (e.g. rocks and soils) as a collection of individual particles bonded together with bonds that have specific stiffness and strength.
(b) DEM automatically detects new interactions of particles by following the internal algorithm, which solves the motion of interacting particles.
(c) As an external force is applied, movements of particles can cause displacement and contact force changes.
(d) Even though some damages occur within a model, these phenomena can be simulated naturally as a form of bond

breakages without re-meshing or additional assumptions.

(e) Individual bond breakage events may coalesce into macroscopic fracture propagation. Thus, the complex non-linear behaviors appear as an emergent feature.

(f) Model scale and particle size are the most critical drawback because of the computational time induced by rich sets of microscopic geometric changes. Depending on computer capability, it may be overcome.

For the past few decades, many researchers have contributed to developing more accurate DEM models in order to give a better understanding for behaviors of rock. Recognized as an appropriate tool for monitoring the entire failure process arising from distinct areas within a model, DEM has been used to analyze the excavation and slope stability problems and hydraulic fracturing simulations for shale gas productions. For example, the effects of injected fluid compressibility and induced fracture propagation during hydraulic fracturing were studied using the fractured model (Damjanac *et al.*, 2010 and Sarmadivaleh *et al.*, 2011). Both model and particle size effects on fracture initiation and reopening process were examined (Gil *et al.*, 2010). DEM is also employed for seismic monitoring induced by hydraulic fracturing (Nabipour *et al.*, 2011) and for many stability problems arising from excavations and slopes (Potyondy and Cundall, 2004 etc.). However, DEM simulation has been mainly applied for isotropic rock despite the fact that role of anisotropic mechanical behaviors of rock is

important in many rock mechanics applications. Therefore, a bonded particle model with smooth joint model is introduced to develop a transversely isotropic rock model. For example, in order to investigate the saturation changes induced by the swell and contract of rock, transversely isotropic material whose constants have been chosen to match the elastic modulus and uniaxial compressive strength from the laboratory experiment was modeled (Potyondy, 2012).

In this thesis, a bonded particle model with smooth joint model is verified using the transformation of compliance tensor in transversely isotropic rock containing one set of fractures, then transversely isotropic rock is modeled to match the anisotropic responses from BTS as well as UCS test. After performing two experiments, failure patterns of disk-shaped and cylindrical specimens are analyzed based on an experimental study on layered rock, which shows that the strength and fracture pattern are dominated by the orientations of layers (Abbass and André, 2010).

1.3 Objectives and Outline of the Thesis

The main objectives of this study are the discrete element modeling of transversely isotropic rock by considering one set of weak planes, represented as the smooth joint model and verification of the effect of smooth joint model on the anisotropic behaviors of its elasticity and strength. As discussed in the previous section, DEM can directly mimic the mechanical behaviors and can exhibit an amount of emergent features of rock. Once the DEM model for anisotropic rock is established, it will able to be applied to other engineering applications affected by the anisotropy of rock such as shale gas hydraulic fracturing, wellbore stability and foundation problems. Moreover, it is possible to apply various researches related with sedimentary rock such as Enhanced Geothermal Systems (EGS) and Carbon Capture and Sequestration (CCS).

This thesis consists of five chapters. Chapter 1 introduces the brief descriptions of transversely isotropic rock and discrete element method and purpose of the thesis. In Chapter 2, the definition of the particulate system of bonded particle model and its calculation cycle are explained in section 1 and 2, and using this model, intact rock modeling was carried out in section 3. The definition and the principle of smooth joint model were described in section 4 and the smooth joint model which has its own microparameters was inserted into the intact rock model (in section 3) so as to characterize the layered model in section 5. Chapter 3 presents the verification of elasticity and strength of transversely isotropic rock and suggests how to determine the

microproperties of smooth joints. The result of DEM modeling for Asan gneiss, Boryeong shale and Yeoncheon schist, and their anisotropic mechanical behaviors are discussed in Chapter 4, followed by conclusions.

Chapter 2. Discrete Element Method

2.1 Bonded Particle Model

As explained by the pioneering work by Potyondy and Cundall (2004), the bonded particle model (BPM) is defined as a dense packing of non-uniform-sized circular or spherical particles jointed at their contact points with parallel bonds and whose mechanical behavior is simulated by the distinct-element method using the two- and three-dimensional discontinuum programs Particle Flow Code (PFC) 2D and 3D, respectively, (Itasca, 2008a, 2008b). Ever since employed to develop a competent numerical model of Lac du Bonnet granite through calibration process, PFC^{2D} has been simulating the mechanical behavior of intact rock by assigning the microparameters in terms of geometry, deformability and strength. The input microparameters are described in Figure 2.1 (Potyondy and Cundall, 2004).

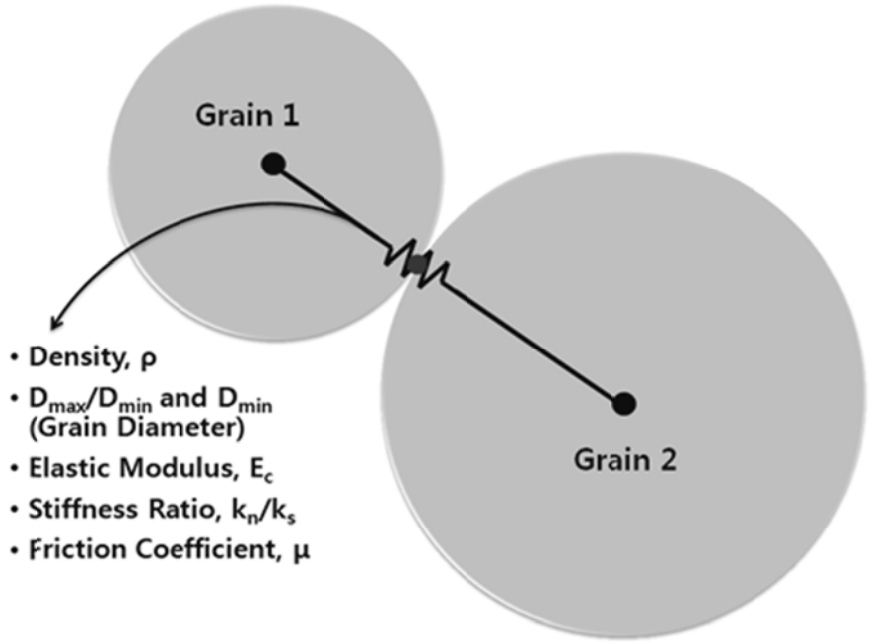

(a) Grain-based Bonding System

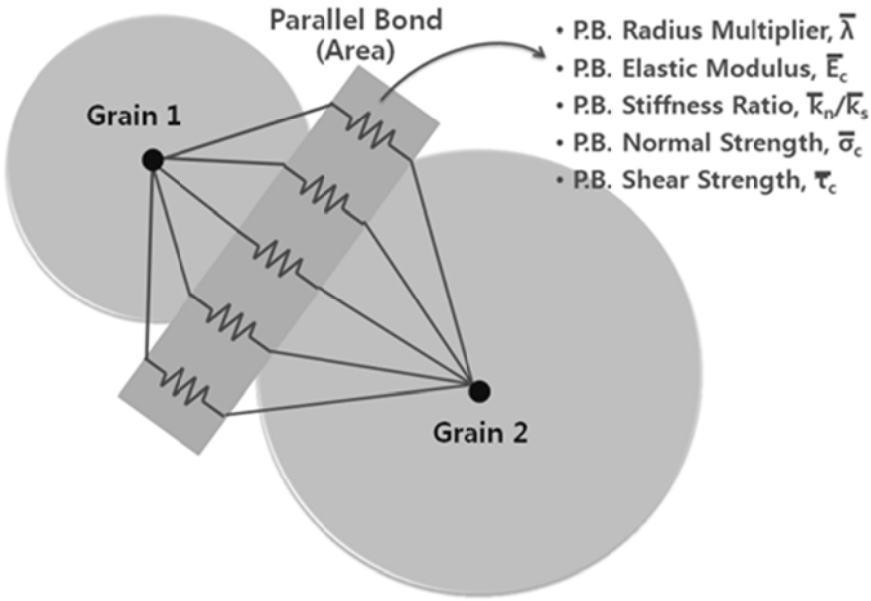

(b) Parallel Bonding System

Figure 2.1: Microparameters of bonded particle assembly

Grain-cement behavior is determined by the microparameters of grains and parallel bonds. The bonding systems are constructed by virtual springs as shown in Figure 2.1. In a grain-based bonding system, normal and shear stiffnesses at a contact point (corresponding to the spring constant) is given by

$$k_n = 2 \cdot t \cdot E_c, \quad t = 1 \tag{2.1}$$

$$k_s = \frac{k_n}{(k_n / k_s)} \tag{2.2}$$

where E_c and t are elastic modulus and unit thickness of grains, respectively and k_n/k_s is the stiffness ratio between grains. In a parallel bonding system, however, normal and shear stiffness are on certain areas (corresponding to the spring constant per unit area) and are given by

$$k_n = \frac{\bar{E}_c}{R^{(A)} + R^{(B)}} \tag{2.3}$$

$$\bar{k}_s = \frac{\bar{k}_n}{(\bar{k}_n / \bar{k}_s)} \tag{2.4}$$

where $\bar{E}_c$ is the elastic modulus of parallel bonds, R is particle radius and $\bar{k}_n / \bar{k}_s$ is the stiffness ratio of parallel bonds. Bonded particles are densely packed and subjected to the material-genesis procedure. Initial assembly is compacted by a material vessel with frictionless planar walls, and the specimen is subjected to the isotropic stress by confining walls. “Floating”

particles that with less than three contact points are removed from the assembly, and parallel bonds are created through all contact points. The material-genesis procedure is terminated by removing the specimen from the material vessel. For calibration, the specimen should be tested under uniaxial/biaxial compression or direct/indirect tension. The calculation cycle triggered from the external compressive or tensile force acting on the specimen is briefly explained in the next section.

2.2 Calculation Cycle

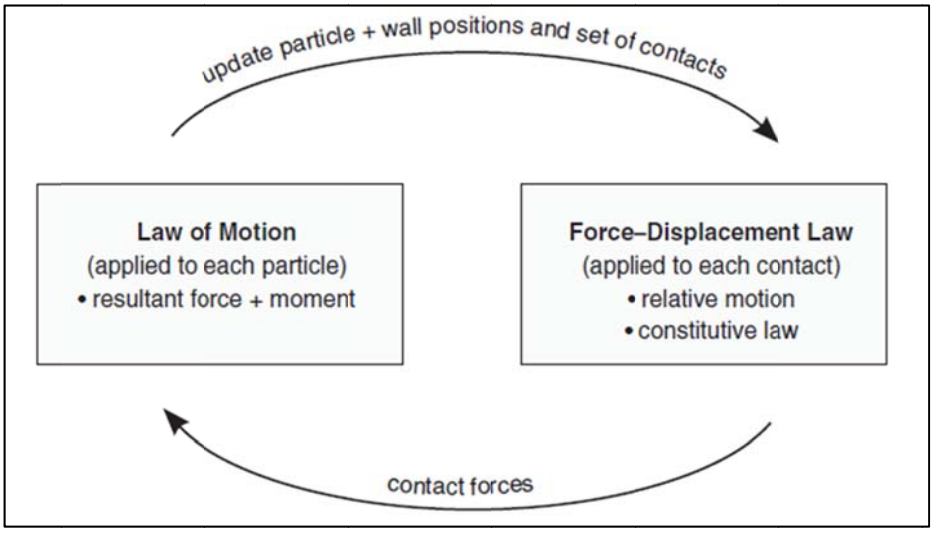

Figure 2.2: Calculation cycle in PFC^{2D} (Itasca, 2008)

Figure 2.2 describes the alternate calculation cycle of the numerical model. Movements and interactions of particles are governed by two basic laws, Newton's second law of motion and force-displacement law, which are expressed as

$$F_e = m \cdot a \tag{2.5}$$

$$F_c = k \cdot u \tag{2.6}$$

When the external force (F_e) is applied to each particle that has a certain mass (m), the acceleration of the particle (a) can be obtained by Newton's second law of motion. By integrating the acceleration, the velocity (v) is obtained; then, if we carry out the integration once again, the displacement of the particle (u) is calculated. Contact force (F_c) can be

calculated by multiplying the stiffness of bonding systems (k) and displacement of particles (u). The calculated contact force (F_c) can work as the new external force (F_e) to the other particles, and the above calculation cycle is repeated.

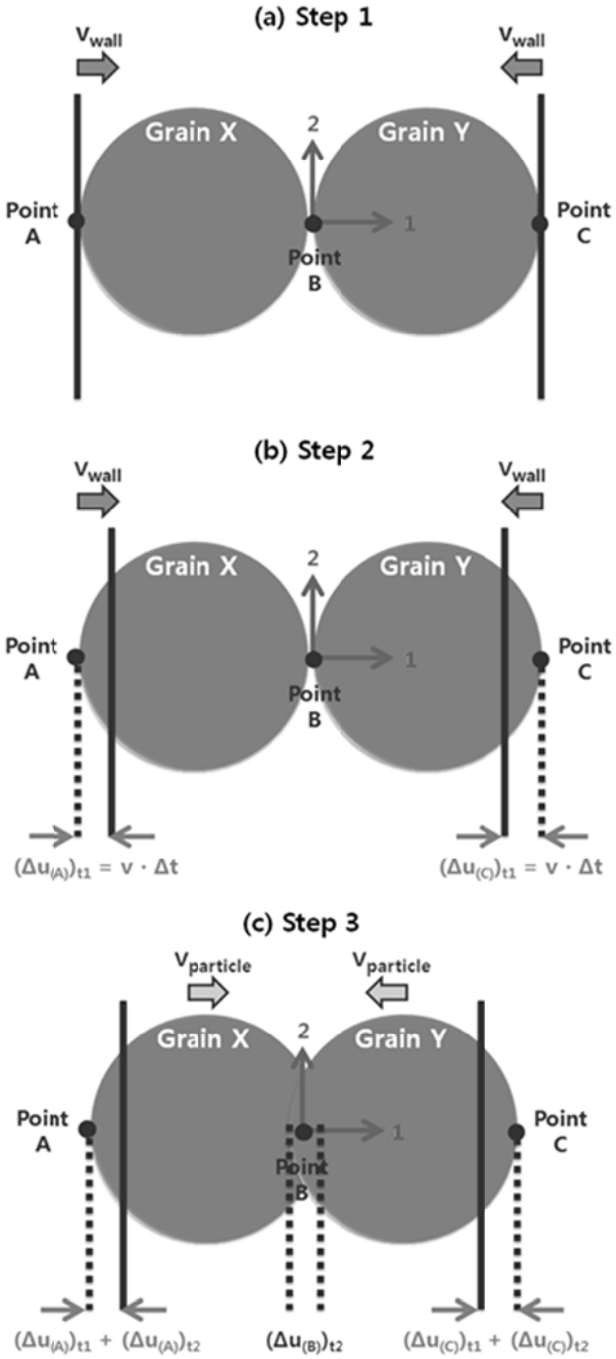

Figure 2.3: Dynamic compression process of two particles. (a) Initial state ($t = t_0$), (b) Moving wall with constant velocity, v and induced displacement ($t = t_1 = t_0 + \Delta t$), (c) Particle movement due to overlap between walls and balls ($t = t_2 = t_0 + 2\Delta t$). (modified from Cundall and Strack, 1979)

The one-dimensional calculation cycle of the bonded particle model is simpler than other implicit models such as finite element methods. The dynamic compression process with respect to time is depicted in Figure 2.3. Provided that a pair of walls moves toward each other with constant velocity (v), walls and particles is overlapped, (displacement, Δu occurs) and then the displacement induces contact normal force (F_n) at each wall-particle contact point in accordance with the force-displacement law.

$$\left(\Delta u\right)_{t1} = v \cdot \Delta t \tag{2.7}$$

$$\Delta F_n = k_n \cdot \cdot \left(\Delta u\right)_{t1} = k_n \cdot v \cdot \Delta t \tag{2.8}$$

$$F_{n,(x)1} = k_n \cdot \left(\Delta u\right)_{t1}, \quad F_{n,(y)1} = -k_n \cdot \left(\Delta u\right)_{t1} \tag{2.9}$$

By Newton's second law of motion, contact normal force (F_n) can be expressed in terms of acceleration (a) and is transformed into an incremental form of velocity of particles (v) by integration. Therefore, another displacement arises from the particles movement with velocity, and the calculation cycles are repeated at the end of the time steps.

$$a_{(x)1} = \frac{F_{n,(x)1}}{m_{(x)}}, \quad a_{(y)1} = \frac{F_{n,(y)1}}{m_{(y)}} \tag{2.10}$$

$$\left[v_{(x)1}\right]_{t2} = \frac{F_{n,(x)1}}{m_{(x)}} \Delta t, \quad \left[v_{(y)1}\right]_{t2} = \frac{F_{n,(y)1}}{m_{(y)}} \Delta t \tag{2.11}$$

$$\left(\Delta u_{(A)}\right)_{t2} = \left\{ v - \left[\frac{F_{n,(x)1}}{m_{(x)}} \right] \cdot \Delta t \right\} \cdot \Delta t \tag{2.12}$$

$$\left(\Delta u_{(B)}\right)_{t2} = \left\{\left[\frac{F_{n,(y)1}}{m_{(y)}}\right]\cdot\Delta t - \left[-v\right]\right\}\cdot\Delta t \tag{2.13}$$

$$\left(\Delta u_{(C)}\right)_{t2} = \left\{\left[\frac{F_{n,(x)1}}{m_{(x)}}\right]\cdot\Delta t - \left[\frac{F_{n,(y)1}}{m_{(y)}}\right]\cdot\Delta t\right\}\cdot\Delta t \tag{2.14}$$

The equations can be expanded to a two-dimensional calculation cycle by introducing the second direction normal to the direction in the one-dimensional model and the components of angular velocities, contact angle between two balls and shear components. Calculation processes regarding the relative rotations of two particles in the two-dimensional model are provided in the references (Cundall and Strack, 1979; Itasca, 2008).

2.3 Modeling of Isotropic Rock

As mentioned in the previous chapter, mechanical properties of Asan gneiss (AS gneiss), Boryeong shale (BR shale), and Yeoncheon schist (YC schist) were used as a reference for numerical modeling. In this section, an intact rock specimen without weak planes, regarded as isotropic rock, was modeled through the BPM, which was calibrated based on the laboratory test results listed in Table 2.1.

Table 2.1: Mechanical properties of AS gneiss, BR shale, and YC schist with resect to the inclined angle (Cho *et al.*, 2012)

Macroproperty		Inclined Angle, β^o [degree]						
		0^o	15^o	30^o	45^o	60^o	75^o	90^o
AS gneiss	E [GPa]	73.53	59.68	58.98	43.90	51.48	57.48	53.77
	UCS [MPa]	223.23	98.57	110.40	111.37	158.83	202.37	183.77
	BTS [MPa]	6.20	8.60	12.43	18.03	18.97	16.67	18.63
BR shale	E [GPa]	42.12	32.53	31.67	27.37	19.57	18.62	23.83
	UCS [MPa]	126.23	96.57	53.50	64.83	83.37	90.97	89.20
	BTS [MPa]	6.40	7.37	8.50	11.27	12.27	13.60	11.10
YC schist	E [GPa]	80.10	58.63	50.58	40.67	26.43	32.37	20.32
	UCS [MPa]	124.77	27.53	27.73	8.93	48.13	119.60	85.00
	BTS [MPa]	2.60	2.87	3.93	4.53	11.33	14.10	17.23

In order to derive isotropic rock properties from the reference, the elastic modulus and strengths that have the least effect of weak planes were selected based on the inclined angles of 0^o and 90^o, respectively.

Following the above discussion, the macroproperties of three isotropic rocks are suggested below:

(a) For elastic modulus on intact rock, the laboratory test results with vertical weak planes are considered to have a minimum effect. Elastic moduli of AS gneiss, BR shale, and YC schist on intact rock were determined as 74, 42, and 80 GPa, respectively.

(b) Uniaxial compressive strength (UCS) on intact rock was chosen as the value on anisotropic rock with horizontal weak planes. The uniaxial compressive strengths of AS gneiss, BR shale, and YC schist used in isotropic calibration were 185, 90, and 85 MPa, respectively.

(c) Brazilian tensile strength (BTS) of AS gneiss, BR shale, and YC schist used in this analysis were approximately 19, 12, and 18 MPa, respectively, which are relatively less influenced by the layered fracture.

Elastic modulus, UCS and BTS of intact rock were determined and the calibrations of intact rocks were conducted by employing BPM. Microproperties (see Table 2.2) such as elastic modulus, stiffness ratio, friction coefficient, and normal and shear strength were chosen to match the

macroscopic behaviors of isotropic rock. Densely packed particle assemblies with ρ = 2650 kg/m^3, D_{max} / D_{min} = 1.66, D_{min} = 0.70 mm, and $\bar{\lambda} = 1$ were set to produce disk-shaped and cylindrical specimens as shown in Figure 2.4. Note that the resolution of assemblies is defined as the number of particles across the specimen width and can be controlled by the particle size. Resolution of assembly generally used in this study is approximately 44 particles across the specimen width.

Table 2.2: Input microproperties for intact rock modeling of AS gneiss, BR shale, and YC schist

Microproperty		Bonded Particle Model		
		AS gneiss	BR shale	YC schist
Grain (particle)	E_c [GPa]	72	38	53
	(k_n/k_s)	4.5	3.5	1.2
	μ	0.839	0.839	0.839
Cement (parallel bond)	$\bar{E}_c$ [GPa]	72	38	53
	$(\bar{k}_n/\bar{k}_s)$	4.5	3.5	1.2
	$\sigma_c = \tau_c$ [MPa]	143	75	80

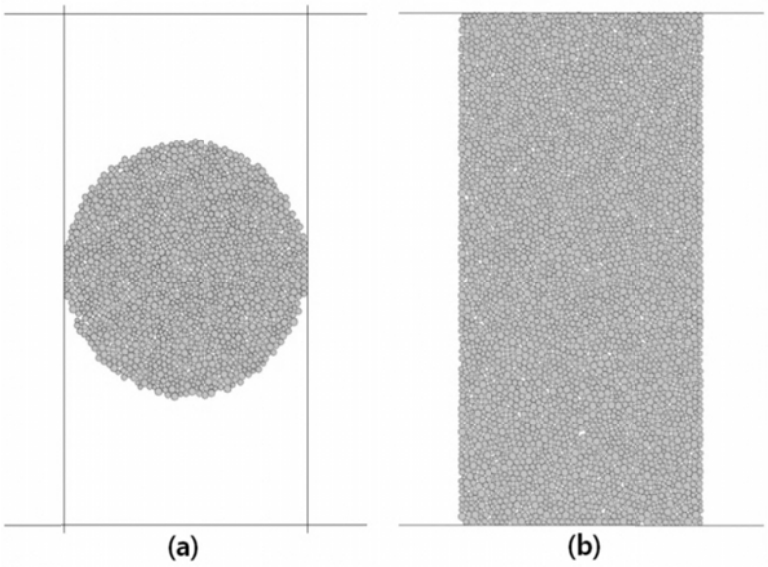

Figure 2.4: Intact rock specimens of resolution 44: (a) disk-shaped specimen for Brazilian test (1554 particles, D = 38 mm) and (b) cylindrical specimen for uniaxial compressive test (3902 particles, 38 mm x 76 mm)

Using two different specimens, BTS and UCS tests were conducted; results from laboratory specimens and bonded particle models are compared in Table 2.3. The results of the numerical model are consistent with those of the laboratory experiment and this agreement indicates that the mechanical behaviors of intact rock were manifest in the bonded particle models. BTS of numerical model for Asan gneiss were slightly overestimated that was also observed in other study, using PFC.

Table 2.3: Macroproperties of laboratory specimens and bonded particle models

Marcoproperty	AS gneiss		BR shale		YC schist	
	LAB	BPM	LAB	BPM	LAB	BPM
E [GPa]	74	76.41	42	43.67	80	81.76
UCS [MPa]	185	189.95	90	88.21	85	90.23
BTS [MPa]	19	43.28	12	19.80	18	20.66

2.4 Smooth Joint Model

The smooth joint model (Mas Ivars *et al*., 2011) simulates the behavior of a smooth interface by ignoring the local particle contact orientations along the original interfaces. Particle pairs lying upon the opposite side of a joint may overlap and "slide" past each other as shown in Figure 2.5. Once the smooth joint is created, pre-existing contact models or parallel bonds are deleted and replaced by smooth joints consisting of newly assigned properties such as dip angle, normal and shear stiffness, friction coefficient, dilation angle, tensile strength and cohesion. The problem arising from the inherent roughness of particles can be solved by inserting smooth joints into bonded particle assembly (Itasca, 2008).

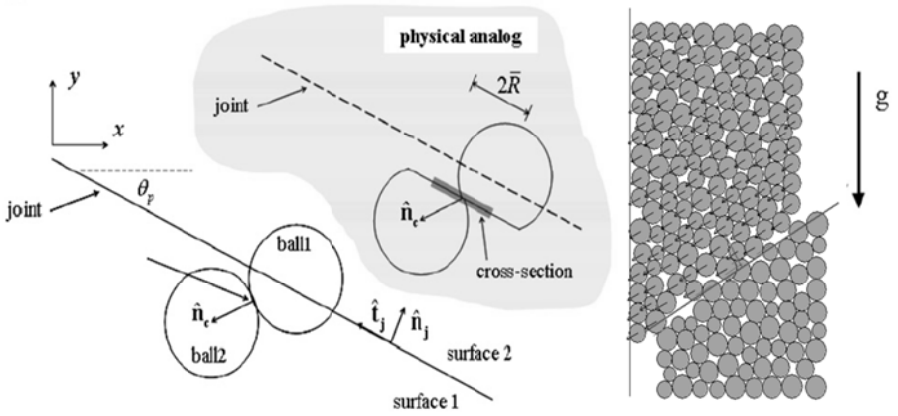

Figure 2.5: (a) Effective joint geometry and (b) 2D specimen with frictionless through-going joint loaded by gravity – large shearing motion results in the creation of new smooth-joint contacts along the joint plane (Mas Ivars *et al.*, 2008)

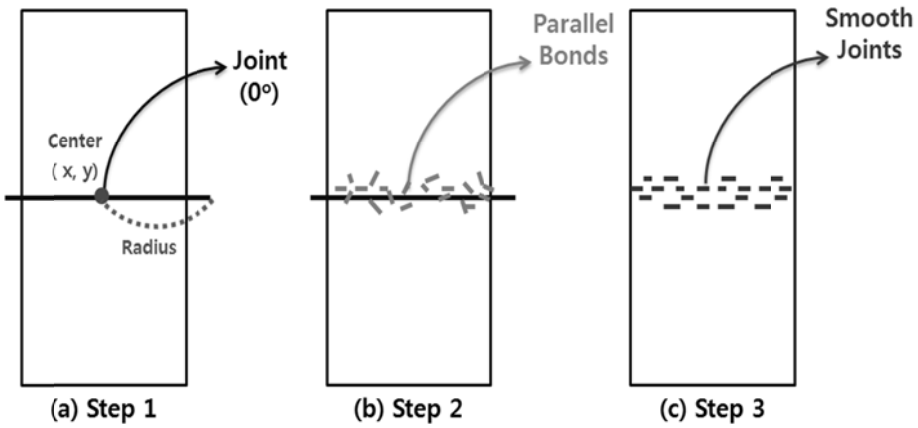

Figure 2.6: Process of smooth joints creation. (a) Determination of joint geometries, (b) finding out the parallel bond that satisfy the criterion of smooth joints at the vicinity of joint, and (c) creation of smooth joints within a bonded particle model

The steps to create the smooth joint model are illustrated in Figure 2.6. First, the joint geometries including center position (x, y, and z components), orientation (inclined angle of normal vector of joint, $\hat{n}_j$ clock-wise from the positive y-axis), and radius are defined. At the same time, the properties of smooth joints containing normal and shear stiffnesses, friction coefficient, dilation angle, tensile strength, and cohesion are assigned. At the vicinity of the joint, parallel bonds that satisfy the criterion of being smooth joint are detected. Finally, these parallel bonds are replaced by smooth joints aligned with joint (Itasca, 2008).

The criterion of smooth joints is depicted in Figure 2.7. In BPM, the center position information of two neighboring balls, *(cen_x1, cen_y1)* and *(cen_x2, cen_y2)* is stored at their contact point. Once the joint geometries and microproperties of the smooth joint are assigned, all contact points are investigated by the fish algorithm to find the parallel bonds that can be

replaced by smooth joints. Eligibility to become a smooth joint is determined by the relative center position of two joined balls located in either the same side or the opposite side of the joint. If the two centers lie on the opposite side of the joint (contacts between balls 1 and 2 or 2 and 5 in Figure 2.7(b)), then the parallel bond at this contact point is eliminated, and a smooth joint is created. If not, the parallel bond remains and keeps its local contact angle and position (contact between balls 1 and 5 in Figure 2.7(b)) (Itasca, 2008).

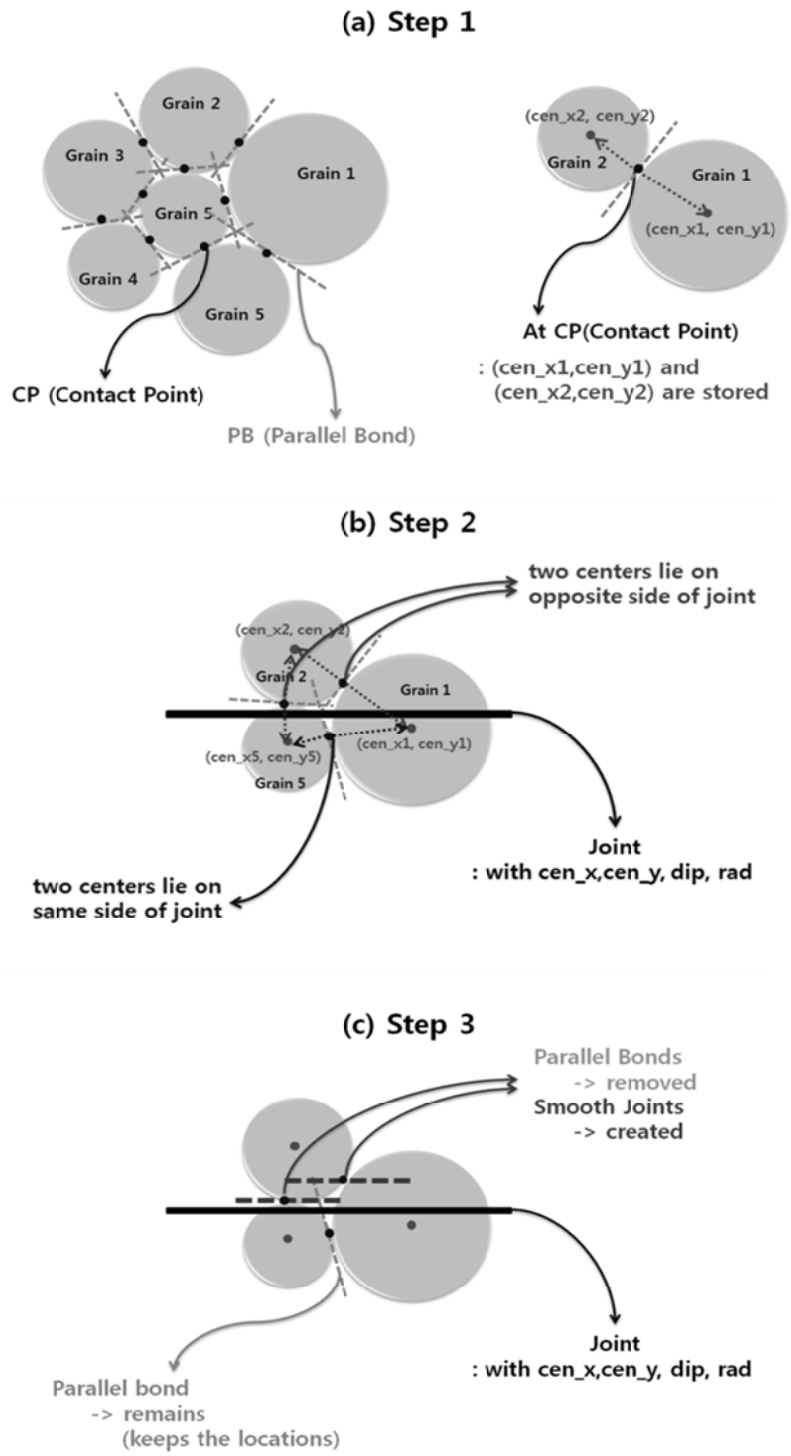

Figure 2.7: Process of the creation of smooth joints by means of the smooth joint criterion. (a) neighboring balls in BPM (b) relative center location lying on either opposite or same side of joint (c) creation of smooth joints

The smooth joint model was originally introduced in order to simulate the behavior of fractured rock mass, so-called Synthetic Roc Mass (SRM), dominated by the strength and elastic properties of fractures. Natural fractures in rock mass are taken into account as a form of discrete fractured network (DFN) model by means of smooth joint models. Even though these fractures are normally separated from each other with very low mechanical properties, this study adopts the smooth joint model to represent weak planes, such as bedding planes, schistosity, and foliations on transversely isotropic rocks. Therefore, the assigned mechanical properties of weak planes should be different from those of fractures. This will be verified in order to confirm that the smooth joints are working competently as weak planes.

2.5 Modeling of Anisotropic Rock

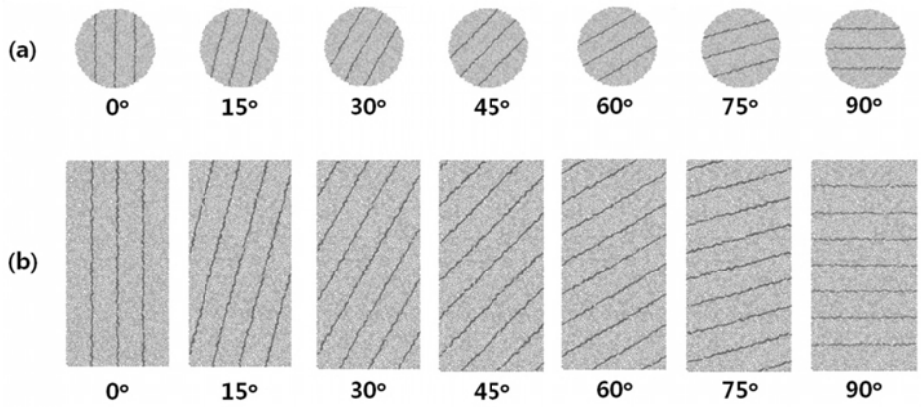

Figure 2.8: Transversely isotropic rock specimens. Smooth joints are inserted into bondad particle model at an 9.5 mm intervals: (a) disk-shaped specimens for the Brazilian test (1554 particles, D = 38 mm) and (b) cylindrical specimens for the uniaxial compressive strength test (3902 particles, 38 mm x 76 mm)

The smooth joints were inserted into the intact rock model (see section 3) to create weak planes in the transversely isotropic rock models. The spacing between each smooth joint was set as 9.5 mm for convenience; seven disk-shaped and cylindrical specimens with inclined smooth joints angles of 0^o, 15^o, 30^o, 45^o, 60^o, 75^o, and 90^o were produced (Figure 2.8).

DEM modeling of layered rock was completed by matching the mechanical properties of the numerical models and experimental results. More detailed procedures on how to determine the microparameters to calibrate both the elastic constant and strengths of numerical models will be discussed in Chapter 4.

Chapter 3. Verification of the DEM Model for Transversely Isotropic Rock

3.1 Elasticity

3.1.1 Equivalent continuum model

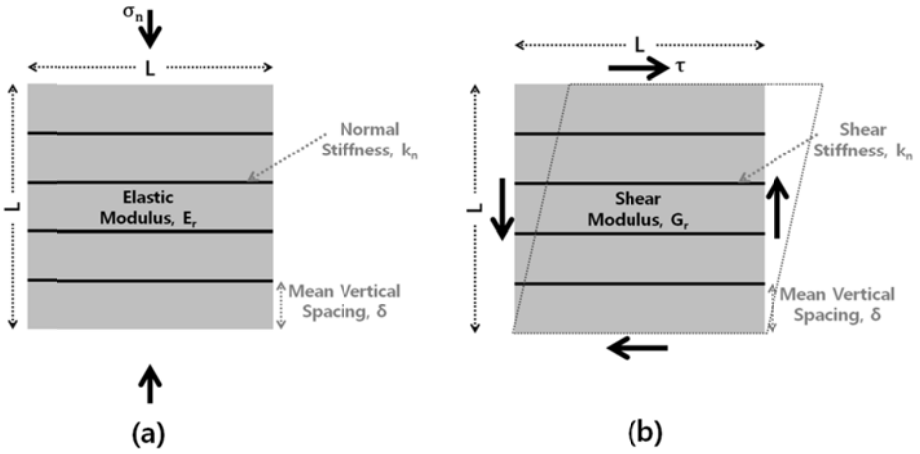

Figure 3.1: Equivalent continuum model containing a single set of horizontal discontinuities for (a) nornal compression and (b) shear displacement (Priest, 1993)

Figure 3.1 is a cross-section of a cubical specimen with side length L embedding a single set of horizontal discontinuities at a mean vertical spacing δ. Note that the specimen contains a total of L/δ horizontal discontinuities. The region of intact rock is assumed to be isotropic material having a constant elastic modulus, E_r, and shear modulus, G_r. A constant normal stiffness, k_n, and shear stiffness, k_s, are placed on discontinuities. When the vertical stress is increased up to σ_n, the specimen is compressed with the vertical

deformation of ΔL, which can be expressed as

$$\Delta L = \left(\frac{L \cdot \sigma_n}{E_r} \right) \tag{3.1}$$

The equivalent elastic modulus (E_e) therefore can be given by

$$\frac{1}{E_e} = \frac{\Delta L}{L \cdot \sigma_n} = \left(\frac{1}{E_r} + \frac{1}{k_n \cdot \delta} \right) \tag{3.2}$$

In the same manner, the horizontal shear displacement ΔH occurs when the pure shear τ is applied parallel to the discontinuities and can be expressed as

$$\Delta H = \left(\frac{L \cdot \tau}{G_r} \right) + \left(\frac{L \cdot \tau}{k_s \cdot \delta} \right) \tag{3.3}$$

Thus the equivalent shear modulus (G_e) can be given by

$$\frac{1}{G_e} = \frac{\Delta L}{L \cdot \tau} = \left(\frac{1}{G_r} + \frac{1}{k_s \cdot \delta} \right) \tag{3.4}$$

The equivalent continuum model is an ideal model for fractured rock mass, because the elastic constants (E_e and G_e) normally used in continuous bodies are defined in the discontinuous model to show the effects of the

properties of discontinuity on anisotropic behaviors of rock. In the case of rock with weak planes, E_e and E_r, can be obtained by conducting the uniaxial compressive strength tests with the maximum load normal and parallel to the weak planes, respectively. In the same manner, G_e and G_r can also be obtained. The optimal spacing with sufficient number of particles between smooth joint can be chosen through iterative process by considering reproduced behavior and computation time. Therefore, the normal and shear stiffnesses of weak planes can be derived from Equation (3.2) and (3.4). The mechanical properties of these discontinuities will provide guidelines on how to evaluate the input microparameters of numerical models.

3.1.2 Compliance tensor

Transverse isotropy with five independent elastic constants is the simplest type of anisotropy and consists of one set of isotropic plane. Based on the generalized Hooke's law, the constitutive equation of anisotropic elastic behavior (Ting, 1996) can be expressed as

$$\varepsilon_{ij} = S_{ijkl}\sigma_{kl} \tag{3.5}$$

where ε_{ij} and σ_{kl} are second-order tensors of strain and stress, respectively, and S_{ijkl} is a fourth-order elastic compliance tensor. By adopting a contracted matrix form, this equation also can be expressed as

$$\begin{bmatrix} \varepsilon_x \\ \varepsilon_y \\ \varepsilon_z \\ \gamma_{yz} \\ \gamma_{xz} \\ \gamma_{xy} \end{bmatrix} = \begin{bmatrix} S_{11} & S_{12} & S_{13} & S_{14} & S_{15} & S_{16} \\ S_{21} & S_{22} & S_{23} & S_{24} & S_{25} & S_{26} \\ S_{31} & S_{32} & S_{33} & S_{34} & S_{35} & S_{36} \\ S_{41} & S_{42} & S_{43} & S_{44} & S_{45} & S_{46} \\ S_{51} & S_{52} & S_{53} & S_{54} & S_{55} & S_{56} \\ S_{61} & S_{62} & S_{63} & S_{64} & S_{65} & S_{66} \end{bmatrix} \begin{bmatrix} \sigma_x \\ \sigma_y \\ \sigma_z \\ \tau_{yz} \\ \tau_{xz} \\ \tau_{xy} \end{bmatrix} \tag{3.6}$$

where S_{ij} is a compliance matrix. The symbols of ε_i, γ_{ij}, σ_i and τ_{ij} (i, j = x, y, z) are normal strain, shear strain, normal stress, and shear stress, respectively. Since the relationship between strains and stresses are subjected to the elastic constants, the compliance matrix can be defined as functions of independent elastic constants. If a material exhibits any physical symmetry, the number of independent constants can be reduced. The symmetry of ε_{ij} and σ_{kl} and the existence of strain energy reduce the total components of independent elastic constants up to 21 in completely anisotropic materials. In the case of transversely isotropic materials, there are only five independent elastic constants (E, E', ν, ν', and G') due to the elastic symmetry of rotation with respect to the y-axis (see Figure 1.1). Thus, the matrix form can be rewritten as

$$\begin{bmatrix} \varepsilon_x \\ \varepsilon_y \\ \varepsilon_z \\ \gamma_{yz} \\ \gamma_{xz} \\ \gamma_{xy} \end{bmatrix} = \begin{bmatrix} \frac{1}{E} & -\frac{\nu'}{E'} & -\frac{\nu}{E} & 0 & 0 & 0 \\ -\frac{\nu'}{E'} & \frac{1}{E'} & -\frac{\nu'}{E'} & 0 & 0 & 0 \\ -\frac{\nu}{E} & -\frac{\nu'}{E'} & \frac{1}{E} & 0 & 0 & 0 \\ 0 & 0 & 0 & \frac{1}{G'} & 0 & 0 \\ 0 & 0 & 0 & 0 & \frac{2(1+\nu)}{E} & 0 \\ 0 & 0 & 0 & 0 & 0 & \frac{1}{G'} \end{bmatrix} \begin{bmatrix} \sigma_x \\ \sigma_y \\ \sigma_z \\ \tau_{yz} \\ \tau_{xz} \\ \tau_{xy} \end{bmatrix} \tag{3.7}$$

For example, S_{22} is the constant that describes the physical meaning of the strain and stress along the y-axis (ε_y and σ_y). The inverse form of the compliance matrix S_{ijkl} is the stiffness matrix C_{ijkl}, which can be regarded as an elastic modulus of transversely isotropic rock.

$$\sigma_{kl} = C_{ijkl}\varepsilon_{ij} \tag{3.8}$$

In laboratory experiments, if the specimen for uniaxial compressive strength test is loaded in the y-direction, the elastic modulus is equal to C_{22} ($=1/S_{22}$). The same manner can be applied to the shear components of S_{44} and S_{66}. By adopting the equivalent continuum model, a new matrix can be derived as follows:

$$\begin{bmatrix} \varepsilon_x \\ \varepsilon_y \\ \varepsilon_z \\ \gamma_{yz} \\ \gamma_{xz} \\ \gamma_{xy} \end{bmatrix} = \begin{bmatrix} \frac{1}{E} & -\frac{\nu'}{E'} & -\frac{\nu}{E} & 0 & 0 & 0 \\ -\frac{\nu'}{E'} & \frac{1}{E}+\frac{1}{k_n \cdot \delta} & -\frac{\nu'}{E'} & 0 & 0 & 0 \\ -\frac{\nu}{E} & -\frac{\nu'}{E'} & \frac{1}{E} & 0 & 0 & 0 \\ 0 & 0 & 0 & \frac{1}{G}+\frac{1}{k_s \cdot \delta} & 0 & 0 \\ 0 & 0 & 0 & 0 & \frac{2(1+\nu)}{E} & 0 \\ 0 & 0 & 0 & 0 & 0 & \frac{1}{G}+\frac{1}{k_s \cdot \delta} \end{bmatrix} \begin{bmatrix} \sigma_x \\ \sigma_y \\ \sigma_z \\ \tau_{yz} \\ \tau_{xz} \\ \tau_{xy} \end{bmatrix} \quad (3.9)$$

where k_n, k_s, and δ are the mechanical properties of discontinuities. The above expressions refer to the stress-strain relationship with respect to the inclined angle of 0^o; note that the inclined angle β is the angle between the maximum loading direction and the surface of parallel discontinuities. This matrix can be generalized in terms of the inclined angle of discontinuities by applying the direction cosines (Ting, 1996):

$$S'_{ijkl} = \beta_{im}\beta_{jn}\beta_{kp}\beta_{lq}S_{mnpq} \quad (3.10)$$

where S_{ijkl} is rotated from the S_{mnpq} using the direction cosines β_{im}, β_{jn}, β_{kp}, and β_{iq} (not the inclined angle of discontinuities) is given by

$$\beta_{ij} = \begin{pmatrix} \cos\varphi & \sin\varphi & 0 \\ -\sin\varphi & \cos\varphi & 0 \\ 0 & 0 & 1 \end{pmatrix} \quad (3.11)$$

The matrix form in Equation (3.10) is not convenient for the calculation of tensor rotation, while the 6 x 6 contracted matrix form requires a relatively simple form of transformation expressed as follows (Lekhnitskii, 1963):

$$S'_{ij} = S_{mn} q_{mi} q_{nj} \tag{3.12}$$

where the direction cosines q_{mi} and q_{nj} are given as

$$q_{ij} = \begin{bmatrix} \cos^2\varphi & \sin^2\varphi & 0 & 0 & 0 & -2\sin\varphi\cos\varphi \\ \sin^2\varphi & \cos^2\varphi & 0 & 0 & 0 & 2\sin\varphi\cos\varphi \\ 0 & 0 & 1 & 0 & 0 & 0 \\ 0 & 0 & 0 & \cos\varphi & \sin\varphi & 0 \\ 0 & 0 & 0 & -\sin\varphi & \cos\varphi & 0 \\ \sin\varphi\cos\varphi & -\sin\varphi\cos\varphi & 0 & 0 & 0 & \cos^2\varphi - \sin^2\varphi \end{bmatrix} = Q \tag{3.13}$$

Consequently, the compliance matrix can be rotated as follows:

$$S' = \begin{bmatrix} c^2 & s^2 & 0 & 0 & 0 & sc \\ s^2 & c^2 & 0 & 0 & 0 & -sc \\ 0 & 0 & 1 & 0 & 0 & 0 \\ 0 & 0 & 0 & c & -s & 0 \\ 0 & 0 & 0 & s & c & 0 \\ -2sc & 2sc & 0 & 0 & 0 & c^2 - s^2 \end{bmatrix}$$

$$\begin{bmatrix} \frac{1}{E} & -\frac{\nu'}{E'} & -\frac{\nu}{E} & 0 & 0 & 0 \\ -\frac{\nu'}{E'} & \frac{1}{E} + \frac{1}{k_n \cdot \delta} & -\frac{\nu'}{E'} & 0 & 0 & 0 \\ -\frac{\nu}{E} & -\frac{\nu'}{E'} & \frac{1}{E} & 0 & 0 & 0 \\ 0 & 0 & 0 & \frac{1}{G} + \frac{1}{k_s \cdot \delta} & 0 & 0 \\ 0 & 0 & 0 & 0 & \frac{2(1+\nu)}{E} & 0 \\ 0 & 0 & 0 & 0 & 0 & \frac{1}{G} + \frac{1}{k_s \cdot \delta} \end{bmatrix} \begin{bmatrix} c^2 & s^2 & 0 & 0 & 0 & -2sc \\ s^2 & c^2 & 0 & 0 & 0 & 2sc \\ 0 & 0 & 1 & 0 & 0 & 0 \\ 0 & 0 & 0 & c & s & 0 \\ 0 & 0 & 0 & -s & c & 0 \\ sc & -sc & 0 & 0 & 0 & c^2 - s^2 \end{bmatrix}$$

(3.14)

Moreover, S'_{22} is expressed as

$$S'_{22} = \frac{1}{E} + \cos^2\varphi \left(\frac{\cos^2\varphi}{k_n \cdot \delta} + \frac{\sin^2\varphi}{k_s \cdot \delta} \right) \tag{3.15}$$

By comparing the elastic modulus obtained by the bonded particle model with the smooth joint model to the component of the compliance matrix (Equation (3.15)), the numerical model was verified in section 3.1.4.

3.1.3 Determination of microparameters

In this thesis, a set of models with varying angles of smooth joints model in the average spacing of 9.5 mm was used in order to verify the smooth joint model in terms of its elasticity and strength behaviors. Referring to the intact

rock properties of Boryeong shale, the model was verified. 38 mm x 76 mm cylindrical specimens were reproduced as numerical models (see Figure 3.2). The elastic modulus of intact rock model is 43.67 GPa as shown in the BR shale results (Table 2.3). The equivalent elastic modulus can be determined as 23.59 GPa. The values of the mean average spacing, δ, the elastic modulus intact rock, E_r, and equivalent continuum model, E_e, were put into equation (3.2); as a result, the magnitude of the normal stiffness, k_n, was calculated as 5400 GPa/m.

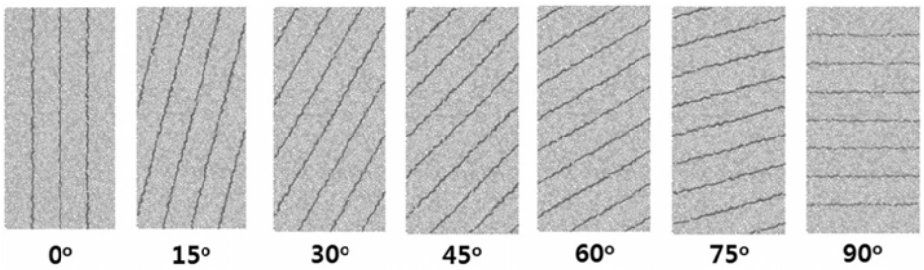

Figure 3.2: A set of models with varying angles of smooth joints model for verification

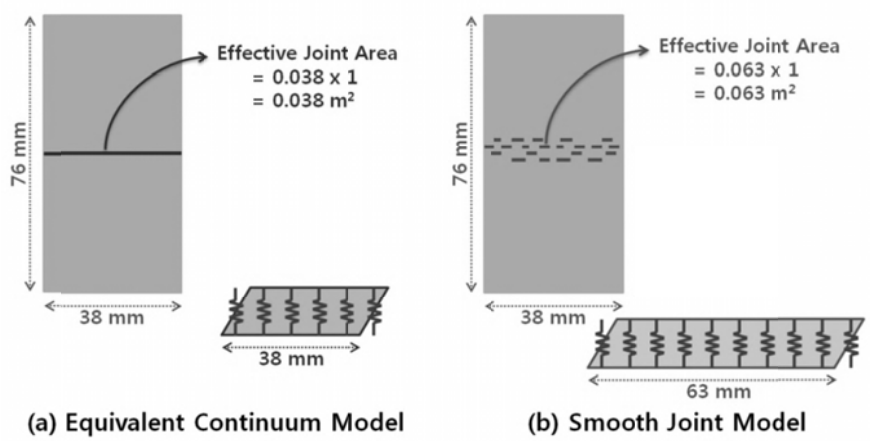

Figure 3.3: Effective joint area of a single joint (a) equivalent continuum model (analytical) and (b) smooth joint model (numerical)

The calculated normal stiffness, 5400 GPa/m, corresponds to the ideal model, which has 38 mm^2 effective single joint area with unit thickness as illustrated in Figure 3.3(a). In the numerical model, however, smooth joints are created by replacing the pre-existing parallel bonds at the adjacent joint, so that the total length of smooth joints cannot be controlled (Figure 3.3(b)). In this study, the total length of smooth joints from single joint is 63 mm, whereas the value of ideal model is 38 mm. Since the dimension of stiffness is Pa/m, stiffer bonding is installed on the smooth joints area (see Figure 3.3). Therefore, reduction in stiffness is necessary to take into account the larger effective joint area in simulated DEM model, in which reduction ratio is the ratio of effective joint area of equivalent continuum model and DEM model. In this study, the reduction ratio is calculated to be approximately 0.6, and the actual input microproperties determined are summarized in table 3.1.

Table 3.2 lists all microparameters of smooth joints used for verification. In order to exclude the effect of rock failure during loading, strength parameters such as tensile strength, cohesion, and friction coefficient were set to be higher than the value of intact rock. Shear stiffness, k_s, of smooth joints varies with the stiffness ratio, K, of 0.2, 0.5, 1.0, 0.2 and 5.0. Here, the stiffness ratio is defined as the ratio of shear stiffness to normal stiffness.

Table 3.1: Input normal sstiffness values, k_n, of equivalent continuum model (analytical) and smooth joint model (numerical) with seven multiple joints

	k_n [GPa/m]	EffectiveArea [m^2]	k_n x Area [GPa·m]
Equivalent Continuum Model	5400	0.266	1440
Smooth Joint Model	3240	0.443	1440

Table 3.2: Input microproperties of the smooth joint model for verification of elasticity

Microproperty	
Normal Stiffness, k_n [GPa/m]	3240 (fixed)
Shear Stiffness, k_s [GPa/m]	648, 1620, 3240, 6480, 16200
Friction Coefficient, μ	57.29 (friction angle = 89^o)
Dilation Angle, Ψ [degree]	0^o
Normal Strength, $\sigma_{n,b}$ [MPa]	100
Cohesion, c_b [MPa]	100

3.1.4 Variation of the elastic modulus in the transversely isotropic model

Using the input microparameters determined in the previous section, the transversely isotropic model is verified. Figure 3.4 shows the variation of the normalized elastic modulus of the smooth joint model. Analytic solution of the elastic modulus with respect to the rotation of axes with different stiffness ratios of weak planes was obtained from the fourth-order stiffness tensor matrix component (Equation (3.15)) by means of tensor transformation using the direction cosine. Elastic moduli were normalized by 43.67 GPa, which is the value of intact rock. Here, the stiffness ratio is defined as k_s/k_n. Note that slightly different notation is in Table 2.2.

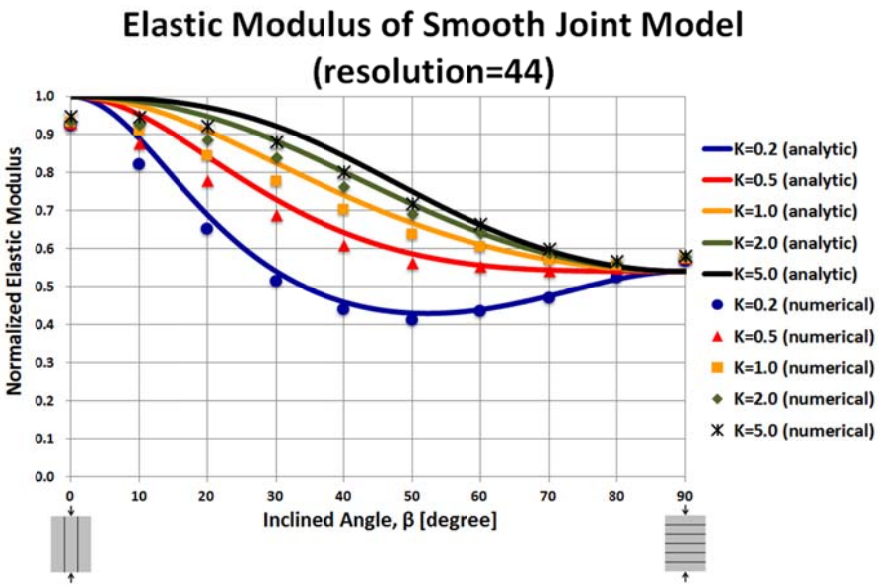

Figure 3.4: Variation of elastic modulus in the transversely isotropic model with stiffness ratio of 0.2, 0.5, 1.0, 2.0, and 5.0

The numerical results show good agreement with the analytic solutions. In the multiple smooth joints model, normalized elastic moduli at the inclined angle of 0^o are slightly less than 1, even though the joints are aligned with the maximum loading direction. This may be affected by the number of vertical joints that have potential to slip according to the smooth joints. The particle size of BPM is also one of the key parameters capable of influencing not only the resolution but also the accuracy of macroproperties.

Table 3.3: Effect of particle size on normalized elastic modulus

Particle size D_{avg} (mm)	Resolution	Total number of particles	Normalized elastic modulus
3.45	11	243	0.704
1.73	22	975	0.762
0.86	44	3902	0.932
0.43	88	15611	0.976

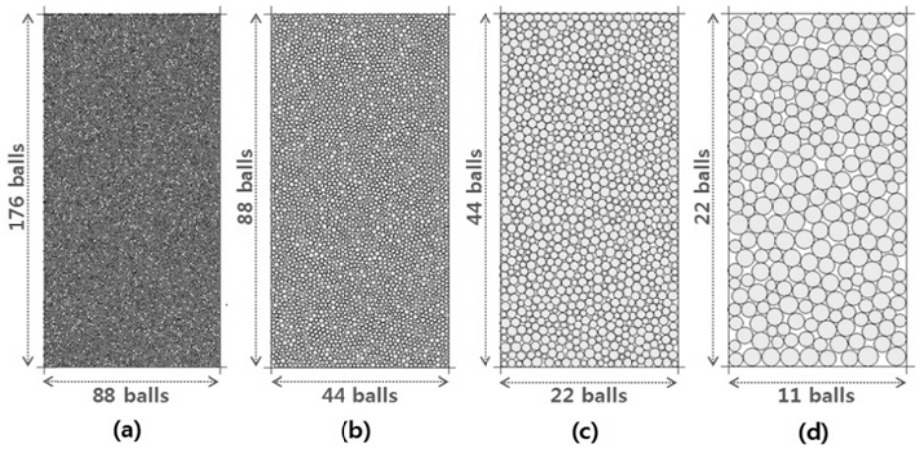

Figure 3.5: Resolutions of the DEM models: (a) 88, (b) 44, (c) 22, and (d) 11 particles

The effect of particle size is clearly seen in Figure 3.6; the particle size, resolution, total number of particles, and elastic modulus with inclined angle of 0^{o} is summarized in Table 3.3. As mentioned in Chapter 2, resolution of assemblies is the number of particles across the specimen width (see Figure 3.5). Depending on the particle size, 11, 22, 44 and 88 particles are generated across the specimen width, and the normalized elastic modulus is close to 1 in the high resolution model. The bonded particle model with smooth joints model can provide a competent tool for simulating the elastic modulus of transversely isotropic rock as long as it maintains a reasonable resolution. Based on this particle size sensitivity analysis, the minimum boundary of resolution and the average particle size in this study are chosen as 22 and 1.73 mm, respectively, since the overall variation of elastic modulus can be matched moderately.

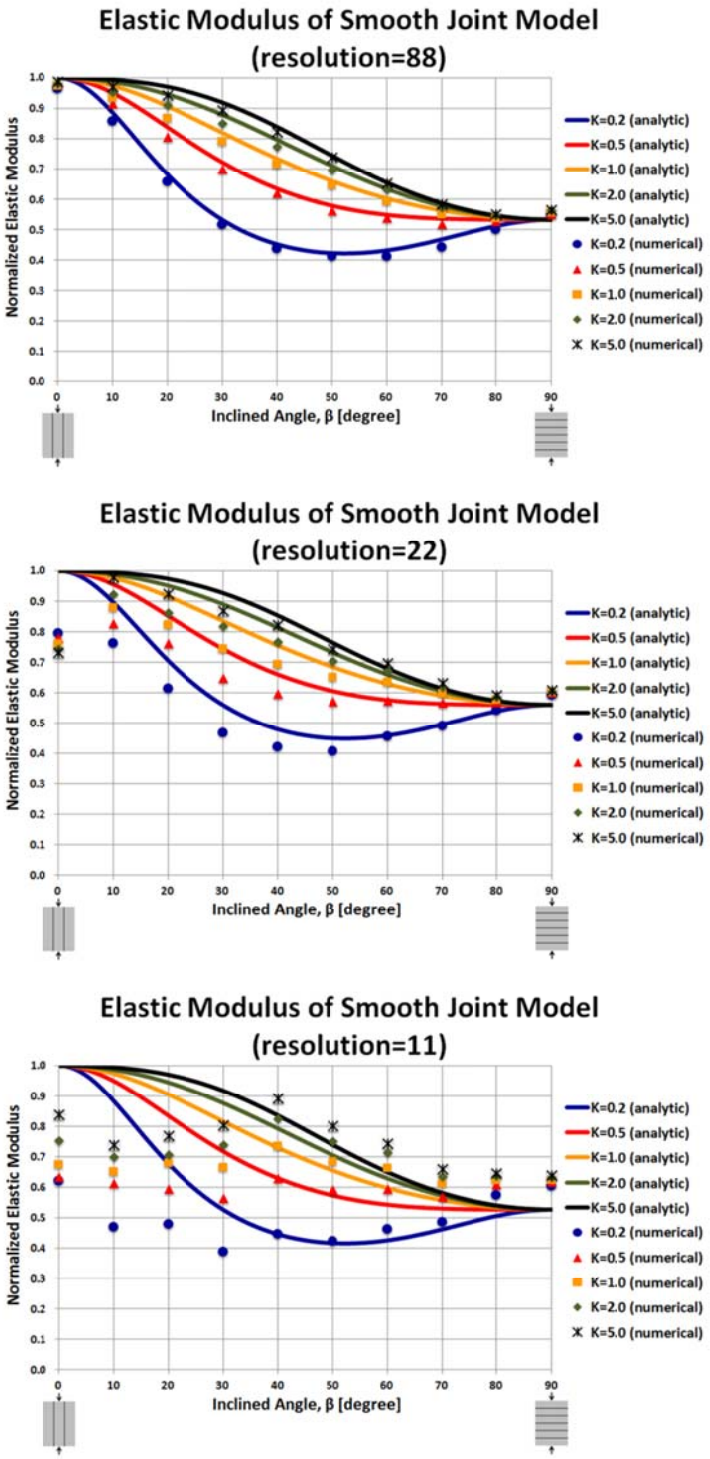

Figure 3.6: Variation of elastic modulus in transversely isotropic model with stiffness ratio of 0.2, 0.5, 1.0, 2.0 and 5.0 with different resolution of 88 (top), 22 (middle) and 11 (bottom)

3.2 Strength

3.2.1 Strength of fractured rock

The strength of fractured rock can be expressed as a function of confining stress, σ'_3; friction angle, φ, and cohesion, C, of rock mass; and the inclination of single set of fractures to the direction of major principal stress, β, as shown below (Jaeger and Cook, 1969):

$$\sigma'_1 = \sigma'_3 + \frac{2 \cdot \left(C'_i + \sigma'_3 \tan \varphi'_i\right)}{(1 - \tan \varphi' \tan \beta) \cdot \sin 2\beta} \tag{3.16}$$

Based on Equation (3.16), a strength curve is presented in Figure 3.7 by cutting-off within an applied major principal stress. Strength curve is an idealized solution, but it still represents the general strength trend of fractured or layered rock. For example, the strength variation of Asan gneiss, Boryeong shale, and Yeoncheon schist also roughly complied with the strength curve. Comparisons of the strengths of the transversely isotropic model and the analytic solution verify the validity of the bonded particle model with the smooth joint model when emulating the strength trends of real rock. Among the microproperties of smooth joint model, the cohesion and friction coefficient (friction angle) can control the strength trends. Thus, other properties such as stiffness are fixed. The parametric studies of cohesion as well as the friction coefficient are discussed in the next section.

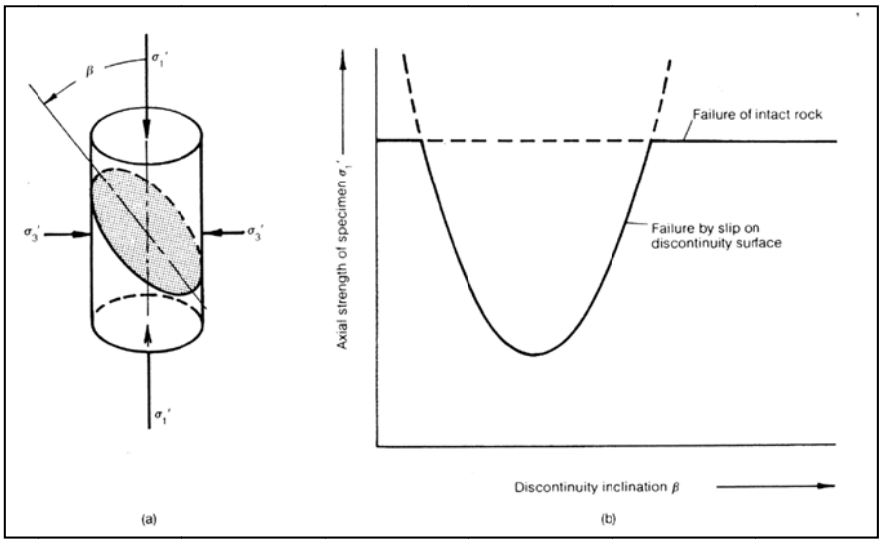

Figure 3.7: (a) Configuration of triaxial test specimens containing a pre-existing discontinuity and (b) strength of specimen predicted by means of equations (Hoek, 1983)

3.2.2 Variation of strength in the transversely isotropic model

Two types of strength variations were investigated by changing the cohesion and friction coefficients condition and fixed friction coefficient. The other microproperties of smooth joint model were fixed as listed in Table 3.4.

Table 3.4: Input microproperties of smooth joint model for verification of strength

Microproperty	
Normal Stiffness, k_n [GPa/m]	3360
Shear Stiffness, k_s [GPa/m]	960
Dilation Angle, ψ [degree]	0^o
Normal Strength, $\sigma_{n,b}$ [MPa]	3
Cohesion, C_i [MPa]	10 (range of 5 to 20)
Friction Angle, φ_i [degree]	20 (range of 0 to 30)

The strength variation with changing friction angle from 0^o to 30^o is presented in Figure 3.8. According to the trend of analytic solutions, the anisotropic behavior is more pronounced with smaller friction angle with wider curve and smaller minimum strength. The DEM model can capture the analytical model to a reasonable extent. As bonded particle model is not a continuum, some discrepancy is inevitably noticed. The DEM model showed that the transition between failure due to the creation of new fracture and existing fracture is not smooth unlike the analytical model, and this in fact shows that the DEM model could be more realistic. Sensitivity analysis of particle size (Figure 3.9) reveals that the numerical model of resolution 11 failed to match the anisotropic strength behaviors. In order to construct a valid numerical model that satisfies the anisotropic strength behaviors, the resolution and average particle size in this study should be at least 22 and 1.73 mm, respectively.

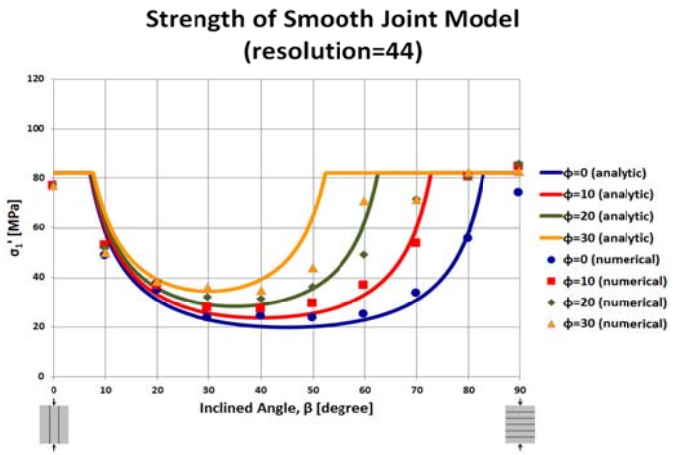

Figure 3.8: Variation of strength in the transversely isotropic model with friction angles of 0^o, 10^o, 20^o and 30^o (cohesion 10 MPa)

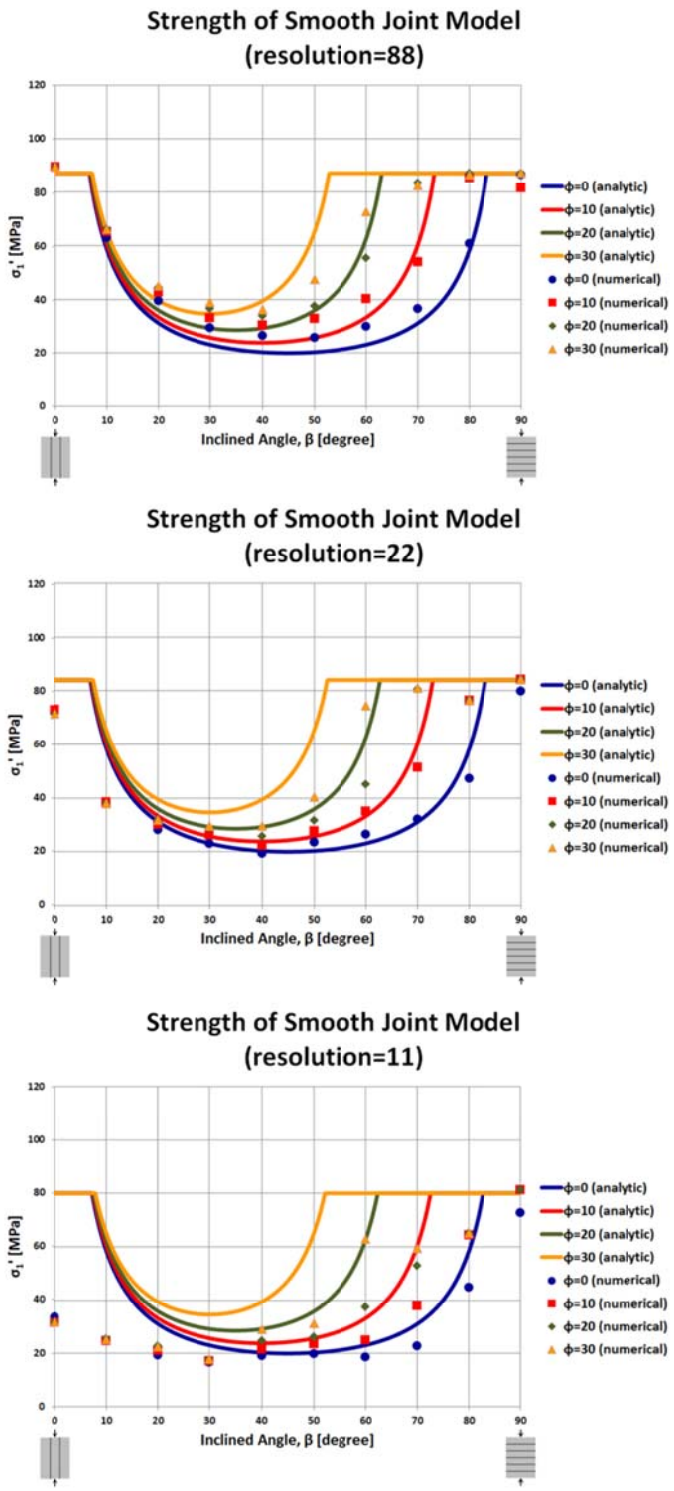

Figure 3.9: Variation of strength in the transversely isotropic model with friction angles of 0^o, 10^o, 20^o and 30^o (cohesion 10 MPa) and resolutions of 88 (top), 22 (middle) and 11 (bottom)

The strength variation with respect to inclined angle was investigated in terms of cohesion ranged from 5 MPa to 20 MPa with intervals of 5MPa (Figure 3.10). When it comes to the trend of analytic solutions, the strength anisotropy is more pronounced with smaller cohesion because of more effect of fractures. The DEM model again captures the effect of cohesion on strength variation. As noted before, there is not a perfect match between analytical and numerical models, however, this is due to the continuum assumptions used in analytical model. The results of particle size sensitivity analysis are represented in Figure 3.11 and as demonstrated in previous case, it confirms that the valid transversely isotropic modeling has to contain the certain amount of particles within a model.

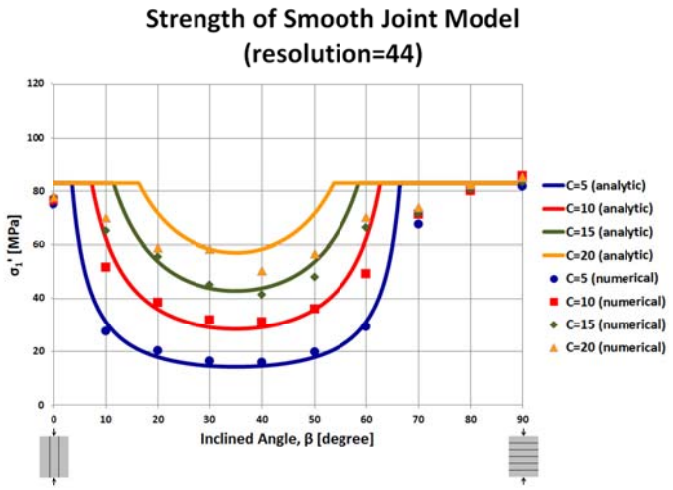

Figure 3.10: Variation of strength in the transversely isotropic model with cohesion of 5 MPa, 10 MPa, 15MPa and 20 MPa (friction angle 20^{o})

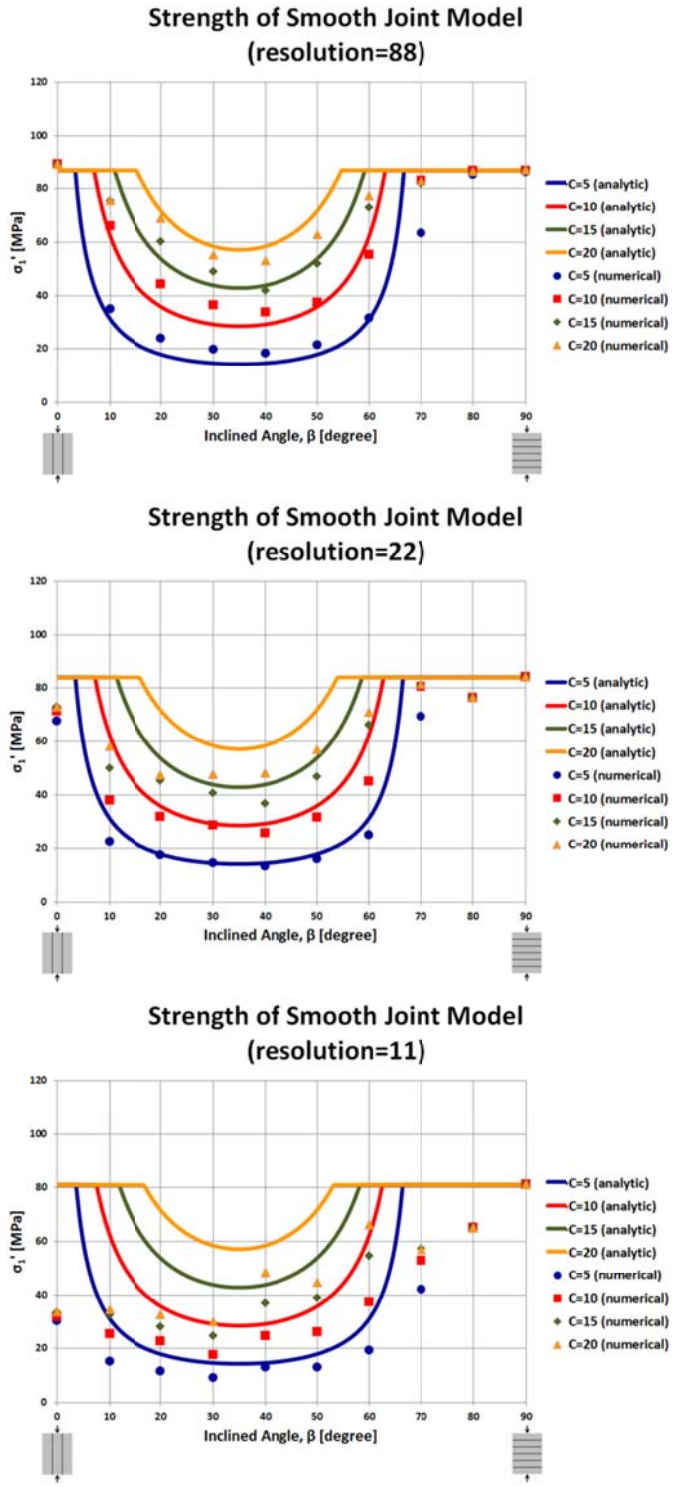

Figure 3.11: Variation of strength in the transversely isotropic model cohesion of 5 MPa, 10 MPa, 15MPa and 20 MPa (friction angle 20°) and resolutions of 88 (top), 22 (middle) and 11 (bottom)

Chapter 4. DEM Model of Transversely Isotropic Rock

4.1 Determination of Microparameters

The microparameters of smooth joints determine the mechanical behavior of joint, and hence that of transversely isotropic mechanical behaviors of transversely isotropic rock. In this section, the procedure to determine these mircoproperties is explained. The properties of Asan gneiss (AS gneiss), Boryeong shale (BR shale), and Yeoncheon schist (YC schist) (Cho *et al.*, 2012) were used as a reference for transversely isotropic rock modeling. In order to consider the layered rock formation consisting of intact rock with weak planes, a bonded particle model with a smooth joint model was adopted in this study. However, the smooth joint model is one of the techniques for representing fractures or joints in rock mass. Thus, the microparameters should be carefully determined; unfortunately, it is difficult to measure the properties of bedding planes, schistosity or foliations of transversely isotropic rock directly through laboratory experiments. As a result, an ideal model (e.g. equivalent continuum model) was introduced to determine the stiffness and microparameters were finalized through iterative process by comparing the laboratory and numerical experiments.

Table 4.1: Normal and shear stiffness of transversely isotropic rocks in the equivalent continuum model

	E_e [GPa]	E_r [GPa]	G_e [GPa]	G_r [GPa]	$k_{n,eq}$ [GPa/m]	$k_{s,eq}$ [GPa/m]
AS gneiss	53.77	76.45	17.10	29.40	19000	4300
BR shale	24.00	43.67	8.70	18.50	5600	1700
YC schist	20.32	81.76	13.70	32.70	2800	2500

In the equivalent continuum model, the normal and shear stiffness of discontinuities can be obtained by considering the elastic constants (E_r, G_r, E_e, and G_e) and the average vertical spacing of weak planes, which were chosen to be 9.5 mm. Normal and shear stiffness of equivalent continuum model ($k_{n,eq}$ and $k_{s,eq}$) were calculated (Table 4.1); based on these values, the stiffness ratio ($k_{n,eq}$ over $k_{s,eq}$) of AS gneiss, BR shale, and YC schist is set as 4.5, 3.5, and 1.2, respectively. As mentioned in Section 3.1.3, because of the difference between the effective joint area in the analytical model and the numerical model, the normal and shear stiffness of equivalent continuum model must be multiplied by the ratio of the analytical joint length to the numerical joint length in order to obtain the normal and shear stiffness of the numerical model ($k_{n,num}$ and $k_{s,num}$).

Weak planes such as bedding planes normally have smooth interfaces without bumpy grains. Hence, the dilation angle (ψ) of discontinuities was regarded as 0^o. In BTS specimens with inclined angle 0^o, the fracturing occurred entirely along the layers and, therefore, it is reasonable to choose the tensile strength of smooth joints as the value less than Brazilian tensile strength with inclined angle 0^o. The friction coefficient (friction angle) and cohesion of weak planes was chosen by iterative process by comparing the

laboratory and numerical experiments. All input microparameters of the smooth joint model (normal and shear stiffness, friction coefficient (friction angle), dilation angle, tensile strength and cohesion) are summarized in Table 4.2.

Table 4.2: Input microparameters of the smooth joint model

Microparameters	AS gneiss	BR shale	YC schist
$k_{n,num}$ [GPa/m]	11450	3370	1730
$k_{s,num}$ [GPa/m]	2540	960	1440
μ (φ)	0.577 (30^o)	0.364 (20^o)	0.268 (15^o)
ψ [degree]	0	0	0
$\sigma_{n,b}$ [MPa]	3	3	2
c_b [MPa]	30	15	10

4.2 Comparison of Laboratory and Numerical Experiments

In this section, three different types of transversely isotropic rock (AS gneiss, BR shale and YC schist) are reproduced as DEM models using the microparameters obtained from the previous section. The calibration results of the numerical experiments are compared with those of the laboratory tests as presented in Figures 4.1, 4.2, and 4.3.

Each Figure presents anisotropic mechanical behaviors in terms of elastic modulus, uniaxial compressive strength, and Brazilian tensile strength. The blue line with triangle indicates the laboratory results, while the red line, yellow-dashed line, and green-dotted line indicate numerical test results with resolutions of 88, 44, and 22, respectively. According to the particle size sensitivity analysis conducted in Chapter 3, the minimum boundary of resolution was derived as 22, so three different resolutions were taken into account. The results demonstrate that the particulate DEM model of transversely isotropic rock can simulate the anisotropic mechanical behaviors of rock. Consideration of anisotropy of rock through the bonded particle model was successful. It is expected that this competent model will be employed in many rock engineering applications.

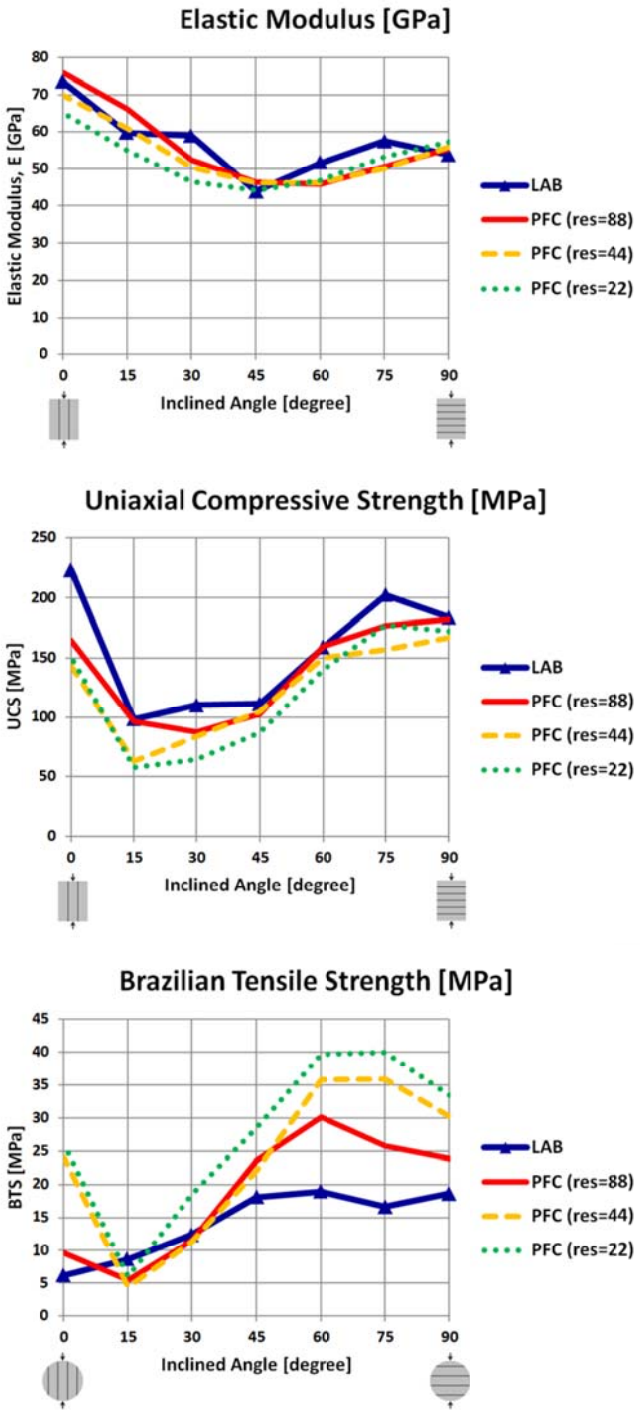

Figure 4.1: Comparisons of elastic modulus (top), uniaxial compressive strength (middle), and Brazilian tensile strength (bottom) between Asan gneiss (laboratory results, blue line) and DEM model (red, yellow-dashed and green-dotted lines)

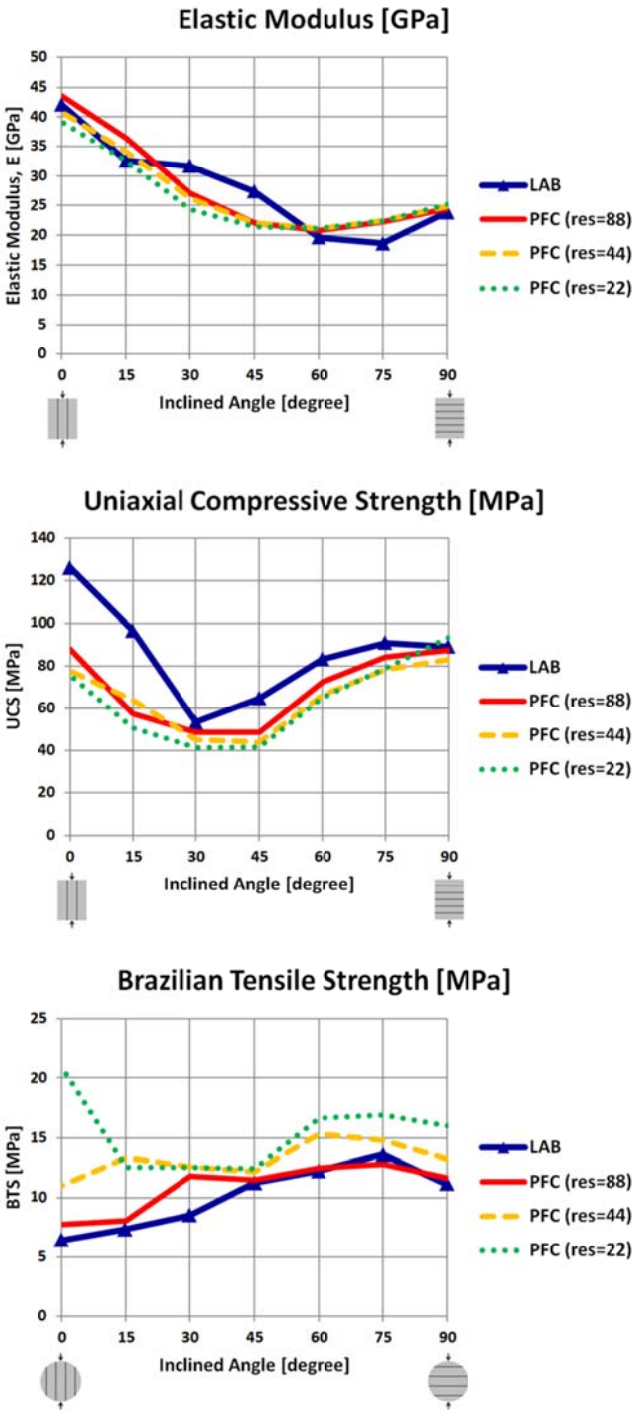

Figure 4.2: Comparisons of elastic modulus (top), uniaxial compressive strength (middle), and Brazilian tensile strength (bottom) between Boryeong shale (laboratory results, blue line) and DEM model (red, yellow-dashed and green-dotted lines

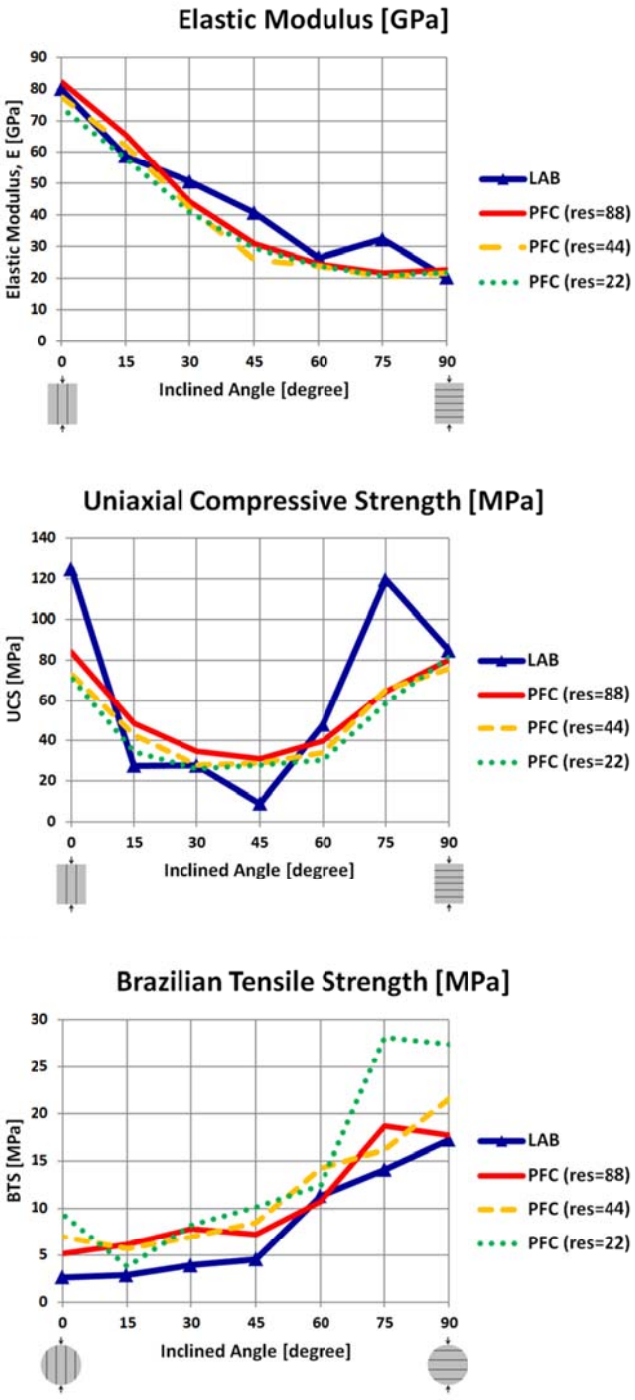

Figure 4.3: Comparisons of elastic modulus (top), uniaxial compressive strength (middle), and Brazilian tensile strength (bottom) between Yeoncheon schist (laboratory results, blue line) and DEM model (red, yellow-dashed and green-dotted lines

As shown in the three Figures, using sufficiently high resolution is one of the key factors that can lead to more accurate DEM modeling. The model with relatively low resolution only captured rough trend of transversely isotropic rock. Generally, the behaviors of the numerical model tend to follow the analytic solutions, especially the elastic modulus. In the laboratory experiment, UCS of the specimen with the vertical weak plane is higher than the value of the specimen with horizontal weak planes. However, this observation cannot be explained in terms of the effect of layers, and therefore, the DEM model cannot address this phenomenon. BTS from DEM modeling tended to be higher than actual value and this has been identified as the inherent limitations, especially for hard rock (Potyondy and Cundall, 2004). It was later known that a clumped bonded particle model can overcome this limitation significantly (Cho *et al.*, 2007). The clumped logic was not employed in this study as the focus was on the capability of smooth joint model in simulating the anisotropic behavior. BTS of the transversely isotropic model with high resolution seems to have good agreement with the laboratory results. Of three types of rocks used in this study, Asan gneiss had less good match which had UCS of larger than 200 MPa. In spite of the issues such as higher tensile strength in strong rock, the DEM model of transversely isotropic rock seems to model the strength and elastic behavior of the transversely isotropic rock to a reasonable extent.

After performing UCS and BTS tests through numerical modeling, the failure mechanism can be analyzed. Failure patterns of Boryeong shale were analyzed as an example, and they are shown in Figures 4.4 and 4.5. In the

numerical models, yellow and cyan are bonded particles and smooth joints, respectively. The breakage of parallel bonds is exhibited as red (tensile) and blue (shear) crack items, and the breakage of smooth joints is represented as magenta (tensile) and black (shear) crack items. As shown in Figures 4.4 and 4.5, the numerical experiments matched well with the laboratory experiments, which mean that the fracture patterns (e.g. fracture initiation and propagation) in both real rock and the numerical model are similar to each other. DEM model can capture failure process of the transversely isotropic rock to reasonable extent and this model can be extended to a larger scale applications.

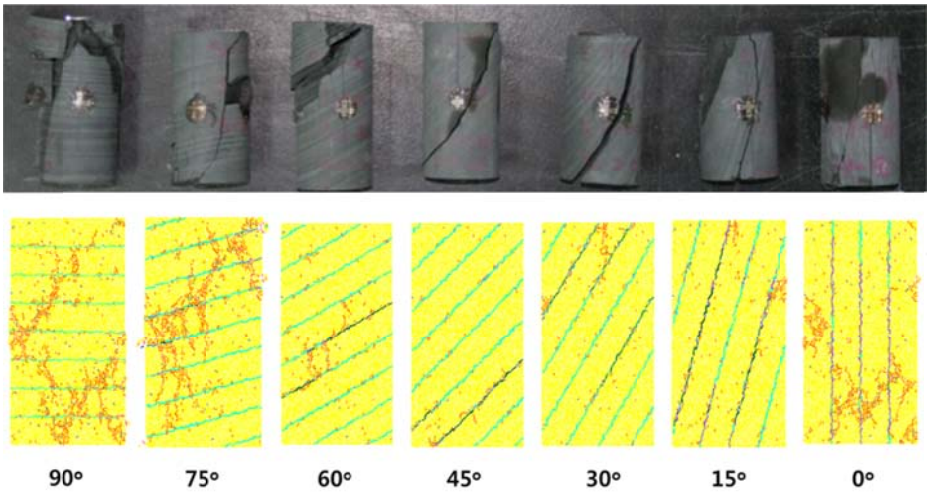

Figure 4.4: Cylindrical specimens after failure in uniaxial compressive strength tests. Boryeong shale (Cho *et al.*, 2012, top) and DEM model (bottom)

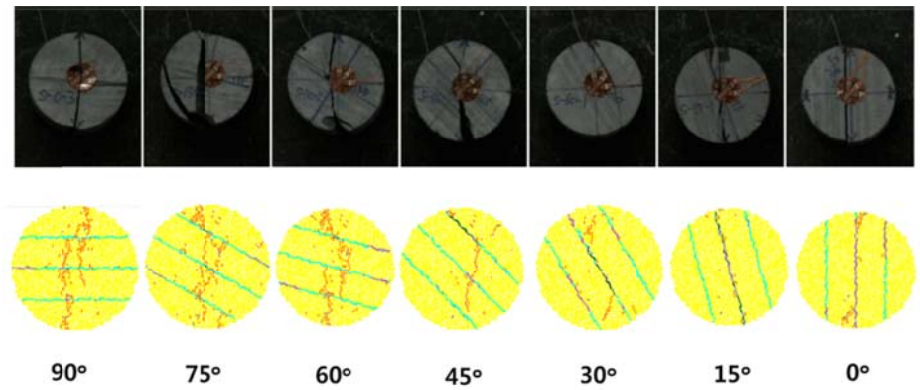

Figure 4.5: Disc-shaped specimens after failure in Brazilian tensile tests. Boryeong shale (Cho *et al.*, 2012, top) and DEM model (bottom)

According to an experimental study of fracture pattern on layered rock (Abbass and André, 2010), the length of all fractures in the specimen, classified as layer activation, central fractures, and non-central fractures (see Figure 4.6), was measured. Note that fractures parallel to the layers are called "layer activation" and some fractures roughly parallel to the loading direction are further called "central fractures" and the rest of fractures are defined as "non-central fracture". The portion of layer activation and central fracture length among total fracture length was calculated (see Figure 4.7).

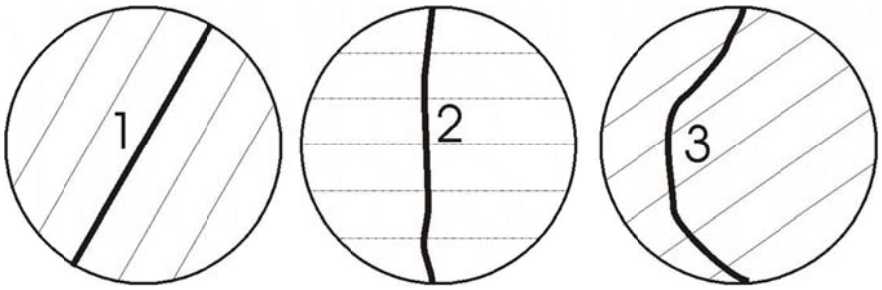

Figure 4.6: Schematic representation of different fracture types in diametrically loaded disks. (1) Layer activation, (2) central fracture and (3) non-central fracture (Abbass and André, 2010)

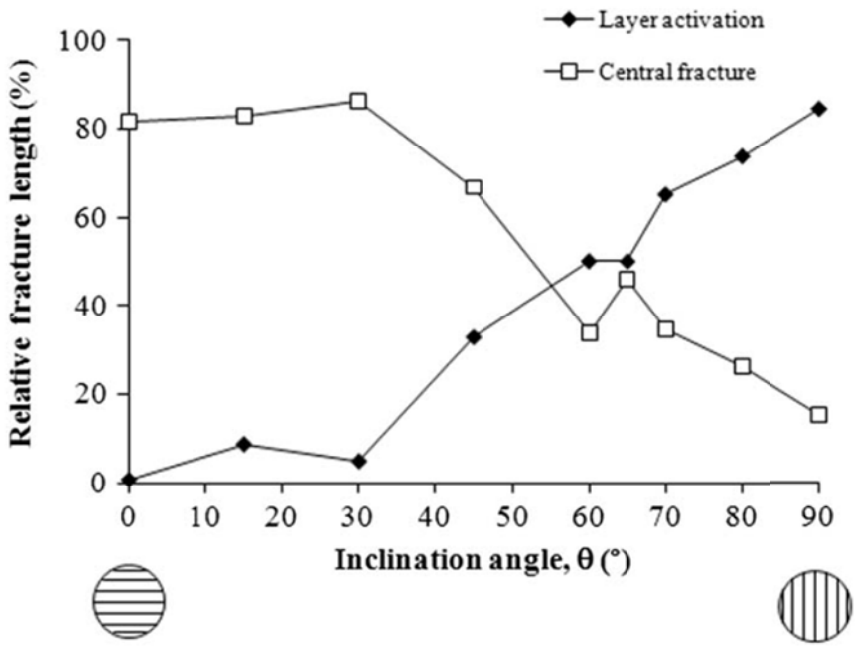

Figure 4.7: Variation in fracture length percentage corresponding to central fracture(s) and layer activation as a function of the inclined angle (Abbass and André, 2010)

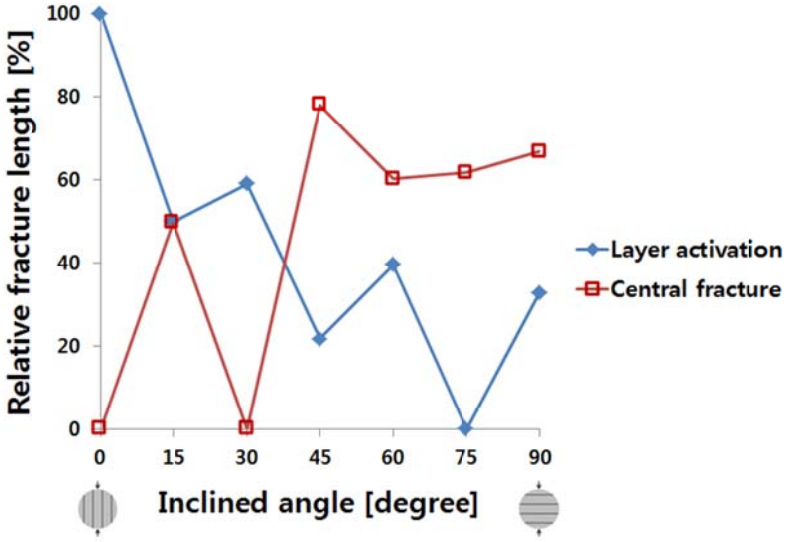

Figure 4.8: Variation in fracture length percentage of Boryeong shale corresponding to central fracture(s) and layer activation with respect to inclined angle

Based on this previous study, each type of fracture on disc-shaped Boryeong shale was measured. As seen in Figure 4.8, the portion of layered fractures at 0^o are 100%, which means the main failure mechanism was tensile failure and the Brazilian tensile strength of Boryeong shale was dominated by that of layers. It is generally analyzed that the strength containing high portion of layered fracture length corresponds to the shear and/or tensile strength of the "layers", while the strength containing high portion of central fracture length corresponds to the shear and/or tensile strength of the "intact materials".

Likewise, the number of micro cracks counted in DEM model can be analyzed to reveal the failure mechanism and is summarized in Table 4.3. According to the total number of micro tensile/shear cracks, it can be analyzed whether the failure mechanism is tensile or shear. In the same manner, the number of micro tensile/shear cracks along with the smooth joints can show the effect of weak planes on the strength and failure mechanism. For example, at the inclined angles of 0^o, 75^o, and 90^o, majority of cracks was tensile cracks, which indicates that the main failure mechanism was tensile failure. Among them, many tensile cracks occurred along the smooth joints at 0^o; thus, the strength might be affected by weak planes. What is interesting many shear cracks observed in angles, 30^o and 45^o. This implies that the main failure mechanisms is not the tensile during BTS test, and this merits further analysis, since BTS is widely used as a method to determining the tensile strength even in anisotropic rock (Amadei, 1996). Therefore, the DEM model can provide a better understanding of the failure mechanisms that contributed to its fail and the magnitude of strength.

Table 4.3: Number of micro tensile and shear cracks induced by UCS and BTS tests in Boryeong shale.

	Inclined Angle	Parallel Bond		Smooth Joint		Total	
		Tensile	Shear	Tensile	Shear	Tensile	Shear
UCS Test	0^o	99	19	96	0	195	19
	15^o	43	7	36	24	79	31
	30^o	14	2	15	15	29	17
	45^o	51	1	16	24	67	25
	60^o	115	11	14	21	129	32
	75^o	232	27	4	1	236	28
	90^o	225	31	2	2	227	33
BTS Test	0^o	9	2	95	0	104	2
	15^o	5	3	8	0	13	3
	30^o	4	1	8	11	12	12
	45^o	6	0	3	0	9	0
	60^o	41	5	1	3	42	8
	75^o	75	6	0	0	75	6
	90^o	26	5	0	0	26	5

Chapter 5. Conclusions

Discrete element modeling of transversely isotropic rock considering one set of weak planes was conducted. The bonded particle model was adopted to construct isotropic material without weak planes, which was calibrated based on elastic modulus and strengths that have least effect of weak planes. The smooth joint model, originally introduced to represent the fractures in rock mass, was used to create the weak planes in this study. Therefore, transversely isotropic rock was represented as the bonded particle model with the smooth joint model with inclusion of smooth joints at intervals of 9.5 mm into the bonded particle model.

In order to verify the effect of the smooth joint model on the elastic and strength anisotropic behaviors, the results of the numerical model and those of the analytical model were compared. Transformation of the compliance tensor in transversely isotropic rock containing one set of weak planes was used as an analytic solution. Variation of the normalized elastic modulus in the numerical model with stiffness ratio of 0.2, 0.5, 1.0, 2.0 and 5.0 showed good agreement with the analytic solutions. Verification with respect to the strength anisotropy also resulted in good agreement with the analytical model. It is demonstrated that the microparameters of the smooth joint model were shown to contribute significantly to the anisotropic mechanical behaviors.

Particle size of bonded particle model is one of the key parameters influencing not only the accuracy of macroproperties. Sensitivity analysis of particle size was carried out during verification in order to determine the

minimum boundary of the particle size (resolution).

Three different types of transversely isotropic rock – Asan gneiss, Boryeong shale, and Yeoncheon schist - were used to be presented by DEM models (Cho *et al.*, 2012). To determine the microproperties of the smooth joint model, the equivalent continuum model was used in order to obtain the normal and shear stiffness of the weak planes. Because of the difference between the effective joint area in the analytical and numerical models, the normal and shear stiffness of the equivalent continuum model were multiplied by the ratio of the analytical joint length to the numerical joint length, which is calculated to be 0.6 in this study. Bedding planes and foliations are generally smooth, so the dilation angle (ψ) was regarded as 0^o. It is reasonable to determine the tensile strength of smooth joints as the value less than Brazilian tensile strength with the inclined angle of 0^o. The cohesion and friction coefficient were estimated through iterative process.

The calibration results of the numerical model with resolutions of 88, 44 and 22 were compared well with those of the laboratory test. Results show that the particulate DEM model of transversely isotropic rock is able to simulate the anisotropic mechanical behaviors of rock. Moreover, the high resolution model can lead to more accurate DEM modeling. By means of weak planes, BTS of transversely isotropic model with high resolution seems to have good agreement with the laboratory results.

The portion of layer activation and central fracture length on Boryeong shale was measured. At inclined angle of 0^o, high portion of layer activation was contained, whereas that of central fractures was contained at inclined

angles of 75^{o} and 90^{o}, which indicate that the strength and the failure mechanism at inclined angle of 0^{o} corresponds to the shear and/or tensile strength of the "intact materials", while the strength and the failure mechanism at inclined angles of 75^{o} and 90^{o} corresponds to the shear and/or tensile strength of the "layers".

Failure patterns in the DEM model were investigated. The breakage of parallel bonds and smooth joints in the numerical model was represented as micro tensile/shear crack items, and the number of micro cracks was counted to distinguish the tensile and shear mechanism. At inclined angles of 0^{o}, 75^{o}, and 90^{o}, an amount of micro tensile cracks were induced, which indicates that the main failure mechanism was tensile failure. Among them, many tensile cracks occurred along smooth joints at 0^{o}. It was concluded that the strength was significantly affected by the weak planes. Shear failure that was often observed in BTS test at angles of 30^{o} and 45^{o} merits further investigation.

In the further studies, the DEM model will be upscaled to engineering applications such as wellbore instability analysis of sedimentary rock and simulation of hydraulic fracturing in the shale gas reservoir. Since rocks in nature are generally anisotropic, the transversely isotropic model developed in this study will pave a way for more accurate analysis by reducing the uncertainty of anisotropy.

Reference

Amadei, B., 1996, Importance of anisotropy when estimating and measuring in situ stresses in rock, *Int. J of Rock Mech, Min Sci. & Geomech.*, 33(3), 293-325.

Amadei, B. and Goodman, R.E., 1981, A 3-D constitutive relation for fractured rock masses, in Proceedings, International Symposium on the mechanical behavior of structured media, Ottawa, Japan, Selvadurai APS (Ed), Part B, pp.249-268.

Barla, G., 1974, Rock anisotropy: Theory and laboratory testing. *In Rock Mechanics,* Müller L. (Ed), 131-169.

Brady, B.H.G. and Brown, E.T., 2004, *Rock mechanics: For underground mining*, Springer.

Cho, J.W., Kim, H., Jeon, S. and Min, K.B., 2012, Deformation and strength anisotropy of Asan gneiss, Boryeong shale, and Yeoncheon schist, *Int. J of Rock Mech & Min Sci.*, 50, 158-169.

Cho, N., Martin, C.D. and Sego, D.C., 2007, A clumped particle model for rock, *Int. J of Rock Mech & Min Sci.*, 44, 997-1010.

Cundall, P.A. and Strack, O.D.L., 1979. A discrete numerical model for granular assemblies. *Geotechnique,* 29(1): 47-65.

Cundall, P.A., 2001. A discontinuous future for numerical modeling in geomechanics? *Geotechnical Engineering,* 149(1):41-47.

Damjanac, B., Gil, I., Pierce, M.E. and Sanchez, M., A new approach to hydraulic fracturing modeling in naturally fractured reservoir, in Proceedings, 44th U.S. Rock Mechanics Symposium, Salt lake city, Utah, Paper No. 10-400.

Davis, R.O. and Selvadurai, A.P.S., 1996, *Elasticity and geomechanics,* Cambridge Univ. Press.

Dusseault, M., and McLennan, J., Massive multi-stage hydraulic fracturing: where are we? *ARMA (American Rock Mechanics Association) e-Newsletter, Winter 2011)*. published, 01/2011.

Fjaer, E., Holt, R.M., Horsrud, P., Raaen, A.M. and Risnes, R., 2008, *Petroleum related rock mechanics 2nd Ed*, Elsevier.

Gil, I., Damjanac, B. and Nagel, N., Geomechanical evaluation of solids injection, in Proceedings, 44th U.S. Rock Mechanics Symposium, Salt lake city, Utah, Paper No. 10-399.

Goodman, R.E., 1989, *Introduction to rock mechanics 2nd Ed,* John Wiley & Sons.

Hoek, E., 1983, Strength of jointed rock masses, *Geotechnique*, 33(3): 187-223.

Itasca Consulting Group Inc., 2008, PFC 2D (Particle Flow Code in 2 Dimensions) Manual, Version 4.0, Minneapolis, Minnesota.

Jaeger, J.C., Cook, N.G.W. and Zimmerman, R.W., 2007, *Fundamentals of rock mechanics*, Wiley-Blackwell.

Jing, L. and Stephansson, O., 2007, *Fundamentals of Discrete Element Methods for Rock Engineering: Theory and Applications*, Elsevier Science.

Lekhnitskii, S.G., 1963, *Theory of elasticity of an anisotropic elastic body*, Holen Day Inc.

Mas Ivars, D., Potyondy, D.O., Pierce, M.E. and Cundall, P.A., 2008, The Smooth-Joint Contact Model (Abstract), in Proceedings, 8th World Congress on Computation Mechanics/5th European Congress on Computational Methods in Applied Sciences & Engineering, Venice, Italy, Schrefler BA and Perego U (Ed), Paper No. a2735.

Mas Ivars, D., Pierce, M.E., Darcel, C., Reyes-Montes, J., Potyondy, D.O., Young, R.P. and Cundall, P.A., 2011, The synthetic rock mass approach for jointed rock mass modeling, *Int. J of Rock Mech & Min Sci.*, 48, 219–244.

Min, K.B. and Jing, L., 2003, Numerical determination of the equivalent elastic compliance tensor for fractured rock masses using the distinct element method, *Int. J of Rock Mech & Min Sci.*, 40, 795-816.

Min, K.B. and Jing, L., 2004, Stress-dependent mechanical properties and bounds of Poisson's ratio for fractured rock masses investigated by a DFN-DEM technique, *Int. J of Rock Mech & Min Sci.*, 41, 390-395.

Okland, D., Hydro, N. and Cook, J.M., 1998, Bedding-related borehole instability in high-angle wells, in Proceedings, EUROCK ’98 – Rock mechanics in petroleum engineering, Trondheim, Norway, Paper No. 47285.

Potyondy, D.O., 2012, The bonded-particle model as a tool for rock mechanics research and application: current trends and future directions, in Proceedings, 7th Asian Rock Mechanics Symposium, Seoul, South Korea, p. 73-105.

Potyondy, D.O. and Cundall, P.A., 2004, A bonded-particle model for rock, *Int. J of Rock Mech & Min Sci.*, 41: 1329-1364.

Priest, S.D., 1993, *Discontinuity analysis for rock engineering*, Chapman & Hall.

Sarmadivaleh, M., Rasouli, V. and Nabipour, A., 2011, A PFC2D simulation of hydraulic fracture and natural interface interaction, in Proceedings, 2nd International FLAC/DEM Symposium, Melbourne, Australia, 379-387.

Tavallali, A. and Vervoort, A., 2010, Effect of layer orientation on the failure of layered sandstone under Brazilian test conditions, *Int. J of Rock Mech & Min Sci.*, 47, 313-322.

Ting, T.C.T., 1996, *Anisotropic elasticity-theory, applications*, Oxford Univ. Press.

Wyllie, D.C., 1999, *Foundations on rock 2nd Ed,* E & FN SPON.

http://ostseis.anl.gov (visited on 16 January 2011)

초 록

대부분의 암석은 층리, 편리 등 다양한 형태의 연약면에 의해 이방적 성질을 갖는다. 하지만 수치모델을 이용한 셰일가스층에서의 수압파쇄나 이방성 암반에서의 보어홀 공벽 안정성 해석 등을 수행함에 있어 해석상의 편의를 위해 이를 등방성이라 가정한 채 해석이 수행되어왔다. 본 연구에서는 이러한 해석 방식의 한계점을 보완하고자 강체로 가정된 원형의 개별입자들로 구성된 입자결합모델에 Smooth Joint Model을 삽입함으로써 암석 내 연약면을 고려한 횡등방성 모델을 제안하였다. 입자결합모델은 강체 입자들이 독립적으로 움직이며 주변 입자와의 접촉 또는 겹침에서 발생한 새로운 힘에 의해 다시 입자가 움직이는 과정을 반복하며 암석의 역학적 거동을 모사하고 있다. 접촉 또는 겸침 시 발생하는 힘은 접촉면에 존재하는 미소 물성값에 의해 결정되는데, 이 값을 조정함으로써 암석의 역학적 거동을 조정할 수 있다. 입자결합모델을 가지고 먼저 등방성 암석을 모사한 뒤, 입자결합모델보다 더 약학 미소 물성값을 갖는 Smooth Joint Model을 입자결함모델 내에 삽입해줌으로써 암석 내 연약면을 모사하고자 하였다. 절리를 모사하기 위한 목적으로 고안된 Smooth Joint Model을 절리가 아닌 층리나 편리 모사에 적용하였으며, 이러한 방식이 적용된 수치모델의 실효성을

검증하고자 횡등방성 암석의 탄성적·강도적 특성에 대한 이론해를 수치모델을 통해 얻은 값과 비교함으로써 그 타당성을 검증하였다. 입자결합모델의 경우 입자의 크기가 수치해석 결과 값의 정확도에 영향을 미치기 때문에 입자 크기의 변화가 횡등방성 모델의 탄성적·강도적 특성에 미치는 영향을 민감도 분석을 통해 알아보았다. 본 연구에서는 수치 모델의 해상도를 가로 길이 38 mm 내에 포함된 입자의 개수로 정의하였으며, 각각 88, 44, 22, 11의 해상도를 갖는 모델을 가지고 민감도 분석을 수행하였다. 그 결과 입자의 크기가 작아 해상도가 큰 횡등방성 모델의 경우에는 수치모델을 통해 얻은 암석의 역학적 물성 값이 이론해를 통해 얻은 값과 비슷한 반면, 입자의 크기가 상대적으로 커 해상도가 낮은 경우에는 수치모델이 암석의 횡등방적 거동을 잘 모사하지 못하는 경향을 보였다. 하지만 일정 수준이상의 해상도를 갖는다면 횡등방성 암석의 거동을 전반적으로 잘 모사하는 것이 확인되었으며 본 연구에서는 해상도 22 이상의 모델에서 암석의 횡등방적 거동이 잘 모사되었다. 검증과정을 통해 Smooth Joint Model의 미소 물성값인 수직/전단 강성, 마찰계수 및 마찰각, 팽창각, 인장강도, 점착력이 암석의 횡등방적 거동 모사에 끼치는 영향이 매우 큼을 알 수 있었다.

실내 암석 이방성 시험결과 얻은 아산 편마암, 보령 셰일, 연천 편암의 탄성계수, 단축압축강도, 간접인장강도를 검증된 모델을

통해 모사하고자 하였다. 수치모델을 이용한 단축압축강도 시험과 간접인장강도 시험 결과 얻은 탄성계수, 단축압축강도 및 간접인장강도가 아산 편마암, 보령 셰일, 연천 편암의 탄성계수, 단축압축강도 및 간접인장강도와 비슷하게 모사하는 것을 통해 제안된 모델이 실제 횡등방성 암석의 역학적 거동을 잘 따르는 것을 확인하였다. 또한 실제 암석과 수치모델을 가지고 수행한 시험 결과 얻은 각각의 파단면 비교하였으며 두 파단면이 매우 비슷하게 일치하는 것을 통해 암석의 파괴 메커니즘에 대하여 분석할 수 있었으며, 암석의 파괴에 연약면이 미치는 영향 또한 분석할 수 있었다. 따라서 본 연구에서 제안된 횡등방성 모델을 층리나 편리를 갖는 암석의 역학적 거동을 모사하기에 적합한 모델임이 확인되었으며, 이는 연약면이 암석의 파괴 메커니즘 및 강도에 미치는 영향을 알아보는데 효과적임을 알 수 있었다. 제안된 횡등방성 모델은 차후 셰일층에서의 수압파쇄 모사나 보어홀 공벽 안정성 해석 등 다양한 분야에 적용될 수 있다는 점에서 이 연구의 의의가 있다.

주요어: 개별요소법, Smooth Joint Model, 이방성 (횡등방성), 보어홀 공벽 안정성, 수압파쇄
학 번: 2011 – 21095